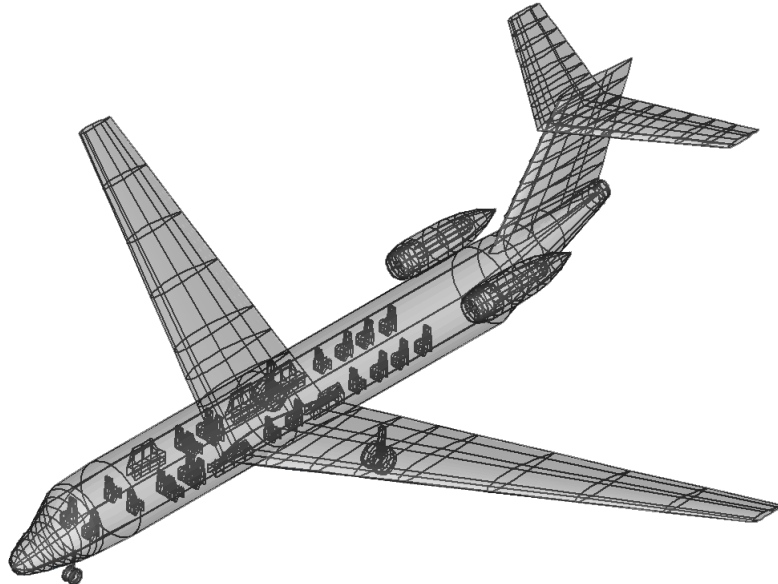




UNIVERSITÀ DEL SALENTO
DEPARTMENT OF ENGINEERING FOR INNOVATION
Master of Science in Aerospace Engineering

AIRCRAFT DESIGN PROJECT REPORT
Conceptual design of a long range business jet:
Scorpion MZ Aircraft



PROFESSOR:
Prof. Giulio AVANZINI

STUDENTS:
Carlo MEO
Andrea ZELINDO

Academic Year 2022-2023

Contents

Abstract	1
1 Introduction	2
1.1 Overview of the design process	2
1.2 The role of business jets in civil aviation	3
1.3 Design requirements	5
1.4 Aircraft data collection and choice of reference airplane	5
2 Preliminary estimation of weights	7
2.1 Empty weight fraction	7
2.2 Payload and crew weight	8
2.3 Fuel weight fraction	8
2.3.1 Sizing mission and historical fuel weight fractions	8
2.3.2 Cruise and loiter weight fraction	9
2.3.3 Parametric analysis for specific fuel consumption and AR values	10
2.4 Takeoff gross weight iterative procedure and parametric analysis results	11
2.5 Final results	13
3 Thrust-to-Weight ratio and Wing Loading	15
3.1 Thrust-to-weight ratio initial estimation	15
3.2 Wing Loading	17
3.2.1 Takeoff	17
3.2.2 Climb	20
3.2.3 Cruise	21
3.2.4 Loiter	22
3.2.5 Landing	22
3.3 Wing loading and Thrust-to-Weight selection	24
4 Initial Sizing and Design Layout	25
4.1 Refined sizing	25
4.2 Fuselage	26
4.3 Wing	28
4.4 Horizontal and Vertical Tail	32
4.5 Engine and Nacelle	34
4.6 Landing gear	36
4.6.1 Main landing gear	37
4.6.2 Nose landing gear	38
4.6.3 Landing gear drag	39
4.7 Design Layout	39

CONTENTS

5 Analysis	45
5.1 Aerodynamic analysis	45
5.2 Cost analysis	53
5.2.1 Airline economic analysis and life cycle cost	57
6 Performance	64
6.1 Takeoff	64
6.2 Climb	66
6.3 Cruise	67
6.4 Landing	67
Bibliography	71

Abstract

This work deals with the conceptual design of a business-class aircraft. In the introduction, the basic aspects of the design process are exposed, followed by the role that the business jet category plays in civil aviation. Moreover, starting from the definition of design requirements, key data from a series of aircraft similar to the one to be sized are shown. A reference aircraft was chosen as a benchmark throughout the entire project in order to derive some missing information needed for sizing and to validate the results obtained.

The initial step of the project involves a preliminary estimation of the weights, based on statistical regressions and basic concepts of flight mechanics. A parametric analysis was performed for the choice of some geometric and propulsive parameters.

Going on with the sizing, the thrust-to-weight ratio and wing loading were defined, through an analysis based on each step of the sizing mission. Again, the key tools were derived from statistics and flight mechanics.

Once the necessary fundamental data were obtained, a review of the initial weights and a preliminary sizing of the main elements of the aircraft (fuselage, wing, tail, engine and landing gear) was possible. The results obtained allow the creation of a desing layout of the aircraft. From the geometry and all the information obtained up to this point, aerodynamic analyses were carried out, in order to redefine preliminary estimates, and economic ones, to establish an aircraft selling price and a rental cost.

Finally, the crucial step of the project is to validate what has been done through a performance analysis, for the purpose of verifying that the requirements imposed have actually been met.

Chapter 1

Introduction

1.1 Overview of the design process

Aircraft design is an iterative process that can be divided into three major phases: conceptual, preliminary, and detail design. The focus of this report is on conceptual design, which involves addressing fundamental questions about configuration, size, weight, and performance. The primary objective of conceptual design is to determine whether it is possible to build an affordable aircraft that meets the given requirements. If not, adjustments to the requirements may be necessary. Conceptual design is a flexible and dynamic process, with new ideas and challenges emerging as the design is explored in more detail.

The starting point of conceptual design is typically either specific design requirements provided by the customer or an estimation of future customer needs. These requirements encompass various aspects such as range, payload, takeoff and landing distances, maneuverability, and speed. Additionally, the design must adhere to a wide range of civil or military specifications. Before commencing the design, decisions need to be made regarding the incorporation of technologies. If the aircraft is intended to be built in the near future, it should rely on currently available technologies, engines, and avionics. However, if the design is for the more distant future, an assessment of emerging technologies is necessary to determine their potential suitability. While advanced technologies may result in a lighter and more cost-effective aircraft for a given mission, they also come with higher development risks.

During conceptual design, a rough sketch is created, illustrating the approximate wing and tail geometries, fuselage shape, and the positioning of major components such as the engine, cockpit, payload/passenger compartment, landing gear, and fuel tanks. This sketch helps estimate aerodynamics and weight fractions through comparisons with previous designs. These estimates are crucial in the process of "sizing," which determines the required total weight and fuel weight for the design mission.

The initial design layout is analyzed to ensure its viability based on the sizing estimates. Detailed calculations involving actual aerodynamics, weights, and propulsion characteristics refine the sizing process. Furthermore, the performance capabilities of the design are evaluated and compared against the specified requirements. Optimization techniques are employed to

identify the lightest or most cost-effective aircraft that can fulfill the design mission while meeting performance criteria.

1.2 The role of business jets in civil aviation

The aim of the project is to develop a high-quality aircraft specifically tailored to meet the needs and preferences of business travelers. The challenges faced by the aviation industry in meeting the growing demand for air travel and the opportunities and benefits of creating a specialized business jet must be considered.

Before delving into the specifics of the project, it is important to understand the context. The aviation industry had long projected an annual growth rate of 3.5 to 5 percent in scheduled airline business prior to the disruptive events of September 11, 2001. However, such unexpected incidents serve as a reminder of the industry's vulnerability to external influences beyond its control, as also evidenced by the events related to the COVID19 pandemic. Despite setbacks, it is anticipated that the industry will recover from periods of recession, resuming the projected growth trajectory.

The projected growth in air travel poses significant challenges for existing airports and associated infrastructure. Many international airports already operate beyond their capacity during peak operating periods, and the expected doubling of demand within the next 15 to 20 years exacerbates the problem. The planning approval and construction timescales for airport expansions are generally incompatible with the pace of demand, leading to concerns about the adequacy of existing facilities.

Moreover, the political, social, and economic factors surrounding airport development projects lie outside the control of the aeronautical industry. Past experiences have shown that planning inquiries and environmental pressure groups have often caused delays in proposed airport expansions. Unfortunately, there is little evidence to suggest that this situation will improve in the future.

To address the capacity limitations at airports, one potential solution is to introduce larger, supercapacity aircraft. However, while this approach may alleviate some challenges, it does not fully resolve the issues arising from increased passenger demand on airport terminal facilities. Accommodating larger aircraft and handling greater numbers of passengers necessitate the expansion of airport infrastructure, including runways, terminals, and other essential services. A critical analysis reveals that over 70 percent of all aircraft movements involve relatively small aircraft, which do not require the same level of services provided at larger airports. Many of these flights serve as regional "feeder" services, connecting passengers to international scheduled services. This mix of small and large capacity services at airports results in an inefficient utilization of available facilities, leading to delays and disruptions.

Business surveys indicate that as passenger demand increases, delays at airports are likely to worsen. These delays and disruptions affect all passengers, including business travelers. While airlines may offer exclusive facilities for business travelers, such as priority boarding and enhanced amenities, these measures do not guarantee the certainty and reliability that

business travelers demand. This situation has prompted some business travelers to explore expensive alternatives, such as using small, exclusive business jets for their journeys. However, this option may not be financially viable for most commercial travelers.

In response to the existing challenges and limitations of the aviation industry, researchers and experts have proposed various solutions. One suggestion is to transfer feeder services to satellite airports, potentially increasing capacity at larger airports without extensive modifications to existing runways and terminal facilities. However, such a shift would necessitate an improved ground transportation system to facilitate seamless transfers between the main and satellite airports. While this concept is slowly being implemented at major hub airports, it is important to consider potential delays and congestion at both airports and the ground interchange.

Capturing the loyalty of business travelers is crucial for the success of any airline. Business travelers typically pay higher prices for their travel compared to tourist-class passengers and provide a more reliable source of income. Offering a differentiated travel experience for business travelers, especially on longer-range flights, has been a common practice. This includes the provision of a separate business-class cabin with larger seats, enhanced in-flight services, dedicated airport lounges, and expedited check-in and luggage retrieval processes. However, specialized all-business-class airlines that exclusively operate smaller aircraft have struggled to attract sufficient customers to achieve profitability. To create an all-business-class airline that appeals to business travelers, numerous factors need to be considered. These include offering larger seats, premium in-flight service, segregation from tourist-class passengers, faster check-in and luggage handling, and minimizing airport delays. Achieving profitability in this market requires filling enough seats on a sufficient number of flights, which may necessitate managed discounts or alternative seating classes. Furthermore, matching the flight frequency of regular airlines is vital to meet the expectations of business travelers.

The successful design and implementation of a business jet project would require careful consideration of all the aforementioned challenges and opportunities. Utilizing aircraft capable of longer ranges and higher speeds, exploring alternative airports, implementing efficient ground transportation systems, and developing innovative business models could potentially address these challenges and make the project commercially viable.

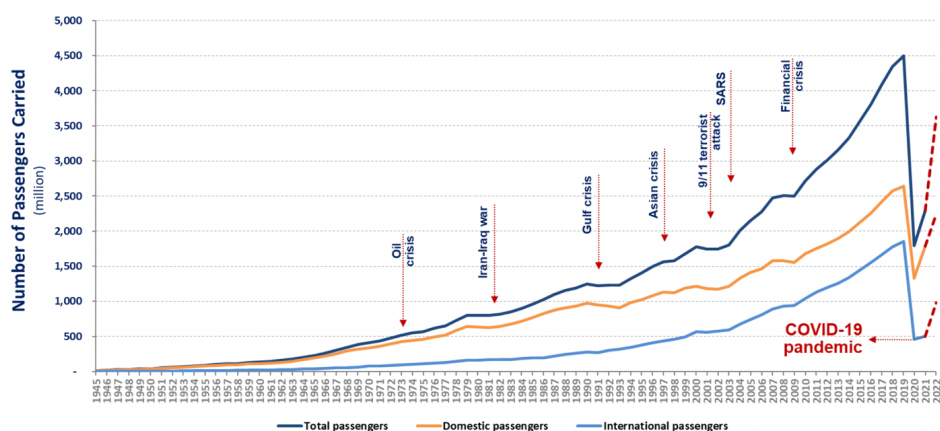


Figure 1.1: World passenger traffic evolution, 1945-2022, ICAO data

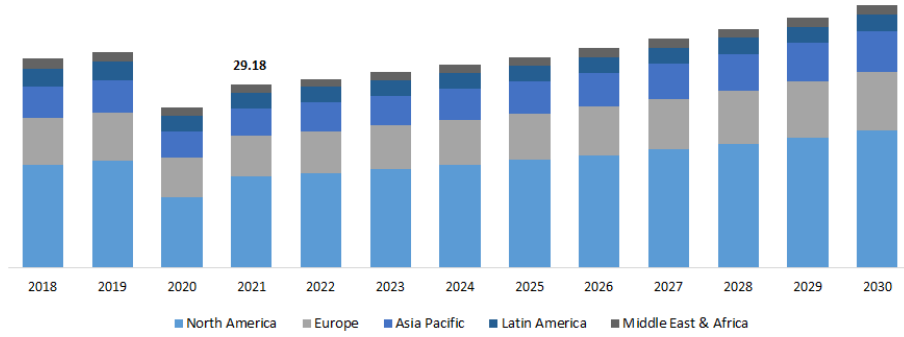


Figure 1.2: Business jet market size by region, 2018-2030, Polaris Market data

1.3 Design requirements

The requirements of the conceptual design of this paper are summarized in the table 1.1. Some values were given according to the units of the British imperial system, others in the international system. All calculations performed are based on the Anglo-Saxon system, however, in order to make interpretation of the results easier, approximated values in the international system will also be provided, keeping in mind that conversion factors often provide additional significant digits.

Requirement	Symbol	Value (SI units)	Value (BE units)
Passengers	N_{pax}	18	18
Range	R	12000 km	6500 nm
Cruise Mach Number	M_{cr}	0.8	0.8
Cruise altitude	h_{cr}	11000 m	36000 ft
Take-off distance required	$TODR$	1500 m	4920 ft

Table 1.1: Initial requirements

1.4 Aircraft data collection and choice of reference airplane

One of the first steps was to collect some useful data related to similar class aircraft in accordance with the defined design requirements. In reviewing the data, a reference aircraft was chosen, consisting of a pre-existing business jet from which useful dimensions, general configurations and all necessary information for preliminary sizing were extracted. Furthermore, the results obtained for each phase of the project were compared with those of the reference aircraft in order to validate the calculations made. The most significant parameters include: the ratio between the wetted and reference surfaces, maximum takeoff weight, operational empty weight, and wing aspect ratio. The aircraft chosen was the Gulfstream Aerospace G650ER, which showed the closest characteristics to the design requirements among all of them. In particular, additional data, related to performance, were found for that aircraft. The data collected are shown below.

Aircraft	MTOW (lb)	W_e (lb)	$W_e/MTOW$	Range (nmi)	N_{pax}	S (ft^2)	b (ft)	AR	E_{max}
Falcon 8X	73000	35730	0.49	6450	14	764	86	9.7	20.2
Global 5500	92500	50306	0.54	5700	16	1023	95	8.8	19.2
Global 6000	99500	51500	0.52	6000	13	1023	100	9.8	20.2
Global 6500	99500	51500	0.52	6600	17	1023	100	9.8	20.2
Gulfstream G550	91000	48000	0.53	6750	19	1001	95	9	19.4
Gulfstream G600	95000	50160	0.53	6500	19	1023	95	8.8	19.2
Gulfstream G650ER	103600	56630	0.52	7000	18	1284	113	9.9	20.4
Gulfstream V	90500	46200	0.51	6500	19	1140	97	8.3	18.6
Average values	93100	48400	0.52	6440	17	1035	98	9.3	19.7

Parameter	Value
S_{wet}/S_{ref} (from CAD)	6.1
$MTOW$	103600 lb
W_e	56630 lb
$W_e/MTOW$	0.52
W_{fuel}	48200 lb
M_{cruise}	0.85
$TODR$	6300 ft
V_{stall}	110 kn
N_{pax}	18
N_{crew}	2
$Range$	7000 nmi
W/S	80.7 lb/ ft^2
T/W	0.38
AR	9.95
S_{ref}	1284 ft^2
b	113 ft
T_{req}	38850 lb

Table 1.3: Reference aircraft: Gulfstream G650ER specs**Table 1.2:** Long range business jets data collection

Chapter 2

Preliminary estimation of weights

The starting point of the conceptual design is the estimation of weights.

Design takeoff gross weight is the total weight of the aircraft as it begins the mission for which it was designed and it can be broken into crew weight, passengers weight, fuel weight, and the remaining empty weight, which includes the structure, engines, landing gear, fixed equipment, avionics, and anything else not considered a part of crew, payload, or fuel. The crew and payload weights are both known since they are given in the design requirements. The only unknowns are the fuel weight and empty weight. However, they are both dependent on the total aircraft weight. Thus an iterative process must be used for aircraft sizing.

$$W_0 = \frac{W_{\text{crew}} + W_{\text{payload}}}{1 - \left(\frac{W_{\text{fuel}}}{W_0}\right) - \left(\frac{W_{\text{empty}}}{W_0}\right)} \quad (2.1)$$

2.1 Empty weight fraction

The empty-weight fraction can be estimated statistically from historical trends as described by Raymer. Table below presents statistical curve-fit equation for Jet transport and its coefficients.

$$\frac{W_e}{W_0} = AW_0^c \quad (2.2)$$

A	c
1.02	-0.06

Table 2.1: Regression exponents for jet transport aircraft

Composite materials are replacing aluminum in many new projects and are a popular design solution nowadays. Raymer's regression is based on data from aircraft predominantly made of classical construction materials, so it was considered correct to pre-multiply the regression formula by a correction coefficient K_c of 0.95, in the case of intensive use of composite materials, because, at the time of publication, not enough composite aircraft had yet been flown to

develop statistical equations. However, by making several attempts for reference aircrafts, it was noted that the classical regression was able to approximate the empty weight and takeoff weight with a sufficient degree of accuracy and was even more accurate than a new regression performed with several more modern aircraft. Based on this observation, considering that the similar aircrafts contain several composite structural elements, both primary and secondary, it was decided not to use the multiplicative coefficient related to the use of composites, so K_c influence was neglected.

2.2 Payload and crew weight

Regarding the total weight of the payload, a weight of 180 lb per passenger was considered, to which a value of 45 lb was added to consider the presence of baggage in the hold. For the crew, considered to consist of one pilot, one co-pilot and two flight attendants, for a total of four crew members, only the weight of 180 lb per individual was considered. This reason derives from the fact that the value of 180 lb represents an average value including the average weight of the individual added to that of a light hand bag. Therefore, if the assumption that the crew travels lighter than the passengers does not occur, however, one heavy bag per passenger was considered, so altogether a total of 810 lb of extra baggage could be loaded in addition to a hand light luggage.

$$\begin{aligned} W_{\text{payload}} &= N_{\text{pax}} \cdot (W_{\text{pax}} + W_{\text{bag}}) = 18 \cdot (180 + 45) = 4050 \text{ lb} \\ W_{\text{crew}} &= N_{\text{crew}} \cdot W_{\text{pax}} = 4 \cdot 180 = 720 \text{ lb} \end{aligned} \tag{2.3}$$

2.3 Fuel weight fraction

2.3.1 Sizing mission and historical fuel weight fractions

The required amount of mission fuel depends upon the mission to be flown, the aerodynamics of the aircraft, and the engine's fuel consumption. As a first approximation, the fuel used can be considered to be proportional to the aircraft weight, so the fuel fraction is approximately independent of aircraft weight. Fuel fraction can be estimated based on the mission to be flown using approximations of the fuel consumption and aerodynamics.

All that remains is to define a sizing mission, divided into several phases, each of which is characterised by its own characteristic weight fraction, defined as the ratio between the weight of the aircraft at the end of the phase and that before the start of the phase in question. The mission is illustrated below.

The weight fractions of the warmup and takeoff, climb and landing phases can be determined by statistical estimates based on historical data, while those relating to the cruise and loiter phases can be estimated by inverting the Breguet equations relating to range and endurance, respectively. The fraction relating to the descent phase is assumed to be 1. Once the mission-segment weight fractions were estimated, by multiplying them together, the total mission weight fraction W_x can be calculated. All weight lost during the mission must be due to

fuel usage. The total fuel fraction can be estimated with the following equation, where a 6% allowance for reserve and trapped fuel was assumed.

$$\frac{W_f}{W_0} = 1.06 \left(1 - \prod_{i=1}^n \frac{W_i}{W_{i-1}} \right) \quad (2.4)$$

The sizing mission consists of the classic phases of take-off, climb, cruise, descent, loiter (with

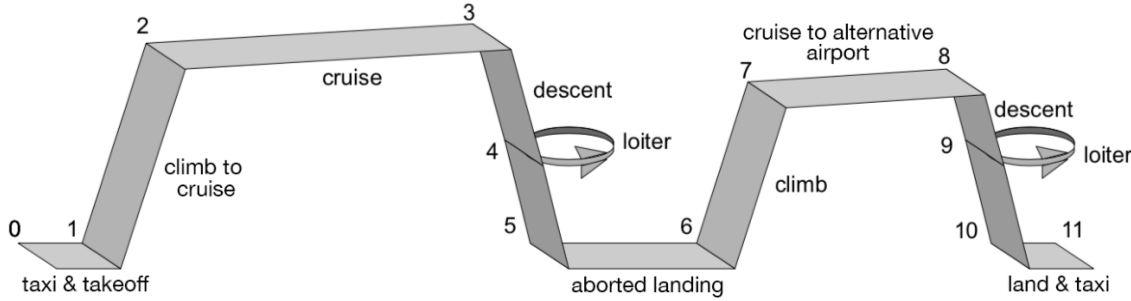


Figure 2.1: Sizing mission profile

a duration of 20 minutes) and landing, to which an additional portion has been added that includes a further climb, a cruise to an alternative airport (defined by a duration of 45 minutes at cruise speed) and again descent, loiter and final landing. This mission does not constitute the typical flight profile, but is a worst-case version of it, in order to size the aircraft in such a way that it can guarantee safe operations in a more severe scenario than the typical one.

Mission fraction	W_i/W_{i-1}
Warmup, taxi and takeoff	0.97
Climb	0.985
Descent	1
Landing	0.995

Table 2.2: Historical mission segment weight fractions for a business jet

2.3.2 Cruise and loiter weight fraction

The Breguet equations used to calculate the weight fractions of cruise and loiter are expressed relatively in the equations 2.5 and 2.6.

$$\frac{W_i}{W_{i-1}} = \exp \left(\frac{-R_{cr} C_{T_{cr}}}{V_{cr} E_{br}} \right) \quad (2.5)$$

$$\frac{W_i}{W_{i-1}} = \exp \left(\frac{-t_{loit} C_{T_{loit}}}{E_{max}} \right) \quad (2.6)$$

It is necessary to point out that the use of best-range and maximum efficiencies, respectively for loiter and cruise, takes for granted the exclusion of the piston-prop and turboprop as engine types for the aircraft under consideration, focusing on jet engines. This choice derives from the

fact that the Mach cruise requirement of 0.8 excludes the possibility of using propeller-driven aircraft, which show a collapse in their efficiency at Mach above 0.6. Moreover, a range of as much as 6500 nmi requires relatively high cruise speeds, so the jet propeller is an unquestionable choice.

The Breguet equations require a preliminary estimate of the maximum efficiency, which can be derived in two ways:

$$E_{max} = \frac{1}{\sqrt{2C_{D0}K}} \quad E_{max} = 15.5 \sqrt{\frac{AR}{S_{wet}/S_{ref}}} \quad (2.7)$$

where the initial estimation of aerodynamic data like C_{D0} and e were assumed to be:

$$C_{D0} = 0.015 \quad e = 0.8 \quad K = \frac{1}{\pi A Re}$$

and S_{wet}/S_{ref} ratio was calculated from a cad model of the reference aircraft, measuring the wetted and reference surfaces, obtaining a value of $S_{wet}/S_{ref} = 6.1$.

The last parameter to be fixed remains the aspect ratio, which is fundamental for design. Although a long, narrow wing with a high aspect ratio has aerodynamic advantages like better lift-to-drag-ratio and improved fuel economy, there are several reasons why not all aircraft have high aspect-ratio wings:

- from a structural point of view, a long wing has higher bending stress for a given load than a short one and therefore requires higher structural-design (architectural and/or material) specifications;
- from a maneuverability perspective, a low AR wing will have a higher roll angular acceleration than one with high AR, because a high aspect-ratio wing has a higher moment of inertia to overcome. In a steady roll, the longer wing gives a higher roll moment because of the longer moment arm of the aileron;
- while high AR wings create less induced drag, they have greater parasitic drag (drag due to shape, frontal area, and surface friction). This is because, for an equal wing area, the average chord (length in the direction of wind travel over the wing) is smaller;
- low aspect ratios have a greater useful internal volume, since the maximum thickness is greater, which can be used to house the fuel tanks, retractable landing gear and other systems;
- for what concerns the airfield size, hangars and other ground equipment define a maximum wingspan, which cannot be exceeded.

2.3.3 Parametric analysis for specific fuel consumption and AR values

The choice of a fixed AR value at this point in the project is a challenging decision, which is the reason for which a parametric analysis was used to identify the best value, at least from

a preliminary dimensioning point of view, for the aspect ratio.

Once all values were defined, the selection of the lowest E_{max} value from the two proposed formulas was chosen, from which the best range efficiency was calculated.

$$E_{br} = \min(E_{max}) \frac{\sqrt{3}}{2} \quad (2.8)$$

Another unknown parameter, at least at this stage of the project, is specific fuel consumption. Here again, Raymer proposes first attempt values for the class of aircraft and engine used. However, even in this case, a parametric approach was opted for, and data was collected on the trend of specific fuel consumption of various turbofan engines over the years.

The parametric analysis performed was based on the choice of the following variation ranges for AR and engine year:

$$AR = 8.5 : 0.1 : 10.5 \quad Year = 2005 : 1 : 2025$$

From these values, the takeoff design weight was calculated for each possible combination using the iterative procedure.

2.4 Takeoff gross weight iterative procedure and parametric analysis results

The parametric procedure was implemented in a MATLAB script by means of two nested 'for' loops:

- an external loop selects one value per round of a vector of maximum efficiencies, calculated from the input vector of ARs; from the selected value, the respective best range efficiency is calculated;
- an internal cycle selects one value per round of a vector of specific consumption, constructed starting from the input vector of engine years supplied as input; to each year, a certain specific consumption is associated, referred to the engine's technological level (turbofans with a BPR around 5 were always considered).

The core of the cycle, namely the operations repeated according to the for conditions, comprises:

- calculation of the weight fractions of each step of the sizing mission, using the equations described in section 2.3.1 and 2.3.2;
- calculation of the fuel weight fraction, using equation 2.4;
- calculation of the empty weight fraction, using statistical regression (eq. 2.2), and of the maximum take-off weight, using equation 2.1; this last phase requires a while cycle, based on the satisfaction of a convergence criterion.

All calculated W_0 s, for each value of E_{max} and C_T , were allocated to a matrix, and

then extracted to calculate the weight, mass and volume of fuel (assuming an average fuel density value of 800 kg/m^3) and empty weight. Finally, matrices were constructed containing the values of W_0 , W_{empty} and W_{fuel} for each combination of E_{max} and C_T , so that the final plots shown in figures 2.2, 2.3, 2.4 could be constructed.

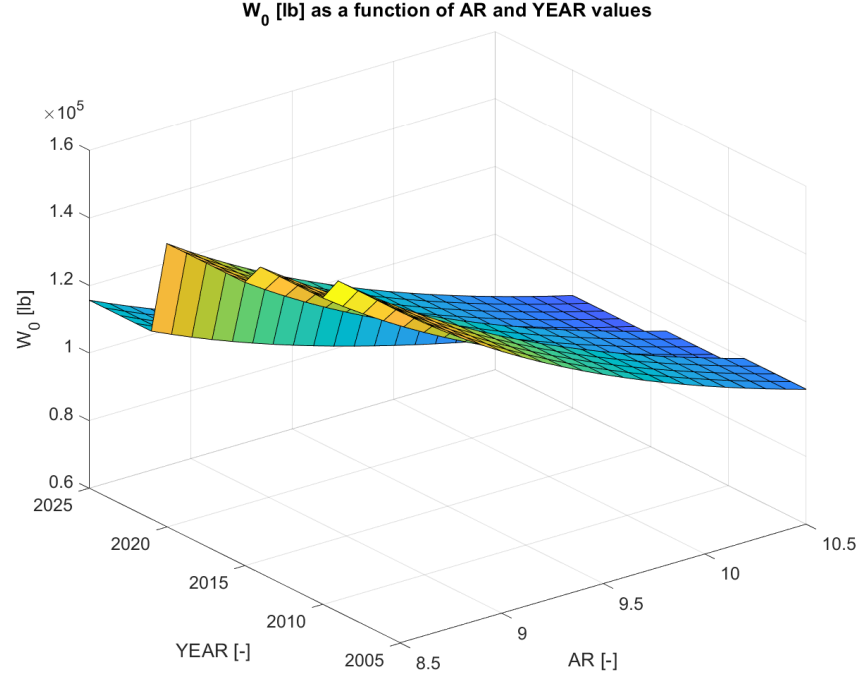


Figure 2.2: W_0 in lb as a function of AR and engine technological level - 3D plot

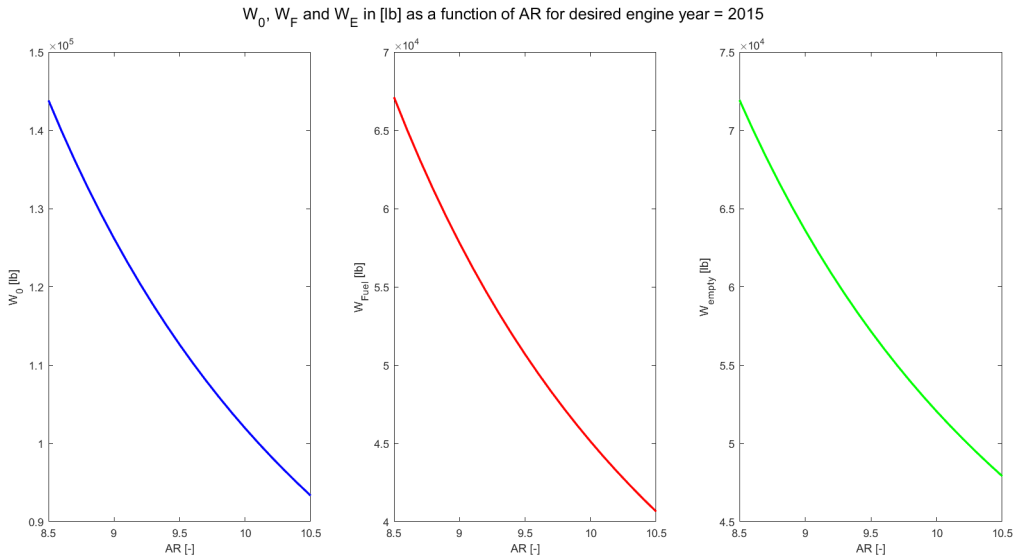


Figure 2.3: W_0 , W_{fuel} and W_{empty} in lb as a function of AR for desidered engine technological level (2015) ($C_T = 0.525 \text{ h}^{-1}$)

Based purely on the theory shown, the results reveal a monotonically decreasing trend of W_0 as AR and engine year increase (which translates into a technological evolution that implies a lowering of specific consumption). Therefore, the optimal choice from a purely take-off weight

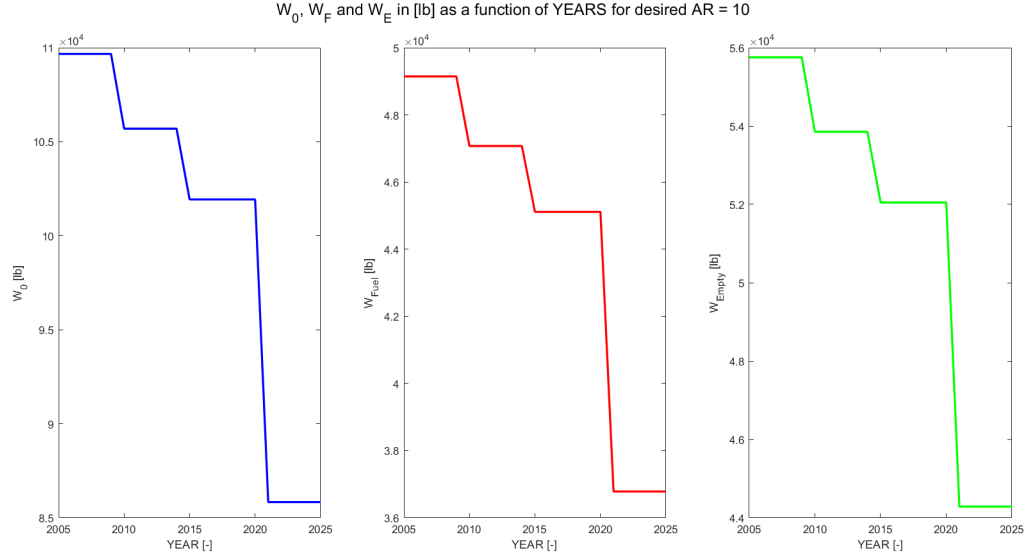


Figure 2.4: W_0 , W_{fuel} and W_{empty} in lb as a function of engine technological level for AR=10

minimisation point of view would be trivial: a higher AR and as new an engine as possible. There are, however, additional factors to consider, linked to economic and construction aspects, which are difficult to include in a parametric conceptual design analysis. Those relating to the choice of AR have been set out in section 2.3.2, while those of the engine can be summarised in the following points:

- a newly designed engine is certainly at the cutting edge from the point of view of performance, implementing innovative technologies that allow it to have better thrust and consumption; however, being a new object without an operating history, the data concerning the reliability discourse is reduced, or even absent;
- an older engine, although less performing, enjoys its accumulated seniority and service experience, in the sense that it is possible to have access to more robust reliability information based on the years.

Furthermore, it is fair to assume that an older engine is more economical than a newly developed one. This discussion will be taken up in the section on the choice of engine approach.

2.5 Final results

Choosing $AR = 10$, and specific fuel consumption values associated with the 2015-2020 technological level corresponding at $C_{T_{cr}} = 0.525h^{-1}$ and $C_{T_{loit}} = 0.425h^{-1}$, the results shown below was obtained. At this point, using the equation 2.4 to calculate the fuel weight fraction and applying the iterative process (as mentioned above) to calculate the empty weight fraction and the maximum take-off weight as reported in 2.1, the following values were obtained:

$$\frac{W_{fuel}}{W_0} = 0.443 \quad \frac{W_{empty}}{W_0} = 0.51 \quad W_0 = 101932 \text{ lb} \quad (2.9)$$

Parameter	Value
AR	10
$C_{T_{cr}}$	$0.525 \text{ } h^{-1}$
$C_{T_{loit}}$	$0.425 \text{ } h^{-1}$
E_{max}	19.85
E_{br}	17.19

Segment	Weight fraction	Value
Warmup, taxi, takeoff	W_1/W_0	0.970
Climb	W_2/W_1	0.985
Cruise	W_3/W_2	0.649
Descent	W_4/W_3	1
Loiter	W_5/W_4	0.993
Aborted landing	W_6/W_5	0.995
Climb	W_7/W_6	0.985
Cruise to AAP	W_8/W_7	0.977
Descent	W_9/W_8	1
Loiter	W_{10}/W_9	0.993
Landing at AAP	W_{11}/W_{10}	0.995

Table 2.3: Mission segment weight fraction

Parameter	Symbol	Value (BE)	Value (SI)
MTOW	W_0	101932 lb	45990 kg
Empty weight	W_e	52049 lb	23610 kg
Fuel weight	W_f	45113 lb	20460 kg
Volume of fuel tanks req.	V_{fuel}	900 ft ³	25.6 m ³
Payload weight	W_{pl}	4050 lb	1840 kg
Crew weight	W_{cr}	720 lb	330 kg

Table 2.4: Main results of preliminary sizing

Chapter 3

Thrust-to-Weight ratio and Wing Loading

The calculation of thrust-to-weight ratio and wing loading travel on parallel tracks and optimisation methods are often used to derive their optimal values. In this chapter, however, reference will be made to the values obtained through first dimensioning methods for calculating the wing loading to meet the various requirements. These allow us to begin the layout with some assurance that the design will not require a complete revision after the aircraft is analyzed and sized. Preliminary values for T/W can be easily derived and were therefore also used in this project. After that, more accurate values for many operational phases can be derived by knowing the wing loading values in each phase.

3.1 Thrust-to-weight ratio initial estimation

The performance of an aircraft is directly influenced by its thrust-to-weight ratio. An higher T/W results in faster acceleration, quicker climb rates, and higher maximum speed. However, larger engines required for higher T/W consume more fuel, increasing the aircraft's takeoff weight to meet the design mission. It's important to note that T/W is not constant. The weight of the aircraft changes during flight due to fuel consumption, and the engine's thrust varies with altitude and velocity and this was taken into account in the calculations. It is crucial to distinguish the takeoff $(T/W)_0$ from T/W at other conditions when performing calculations. If a required ratio is calculated at a different condition, it must be adjusted back to takeoff conditions to determine the number and size of the engines needed.

As suggested by Raymer, a typical value for T/W for a jet transport is 0.25. T/W is also closely related to the maximum speed of the aircraft through the equation 3.2. At this stage of the project, curve-fit equations based on the maximum Mach number can provide an initial estimation of T/W where a is equal to 0.267 and C is equal to 0.363. A M_{max} of 0.9 was considered, based on an approximate 10% increase in Mach cruise and considering the top speed of several similar business jets, obtaining a T/W equal to 0.257.

To obtain a more accurate initial estimate of the required T/W for aircraft designed with

a focus on cruise efficiency, "thrust matching" can be utilized. This involves comparing the selected engine's thrust available during cruise to the estimated aircraft drag. In level unaccelerating flight, the thrust must be equal to the drag. Similarly, the weight must be equal to the lift. Consequently, the T/W ratio must equal the inverse of the lift-to-drag ratio (L/D) as can be seen from the equation 3.3.

$$\left(\frac{T}{W_0}\right)_{\text{typical}} = 0.25 \quad (3.1)$$

$$\left(\frac{T}{W_0}\right)_{\text{statistical}} = aM_{max}^C = 0.267 \cdot 0.9^{0.363} = 0.257 \quad (3.2)$$

$$\left(\frac{T}{W}\right)_{\text{cruise}} = \frac{1}{(L/D)_{\text{cruise}}} = 0.0582 \quad (3.3)$$

The last value obtained in 3.3 must obviously be scaled to the takeoff conditions for the reasons already stated as shown in 3.4. The ratio of the weights is known from the analyses already carried out in the previous chapter, the only unknown is the thrust lapse rate ($T_{\text{takeoff}}/T_{\text{cruise}}$). This value was then derived from the characteristic curves in Appendix A4 [1] (and shown in figure 3.1) which relate the thrust values of a medium bypass ratio turbofan to the flight altitude and flight Mach number. This procedure will also be repeated thereafter whenever it is necessary to scale the thrust-to-weight ratio to the take-off condition (of course with the correct weight ratio and lapse rate values).

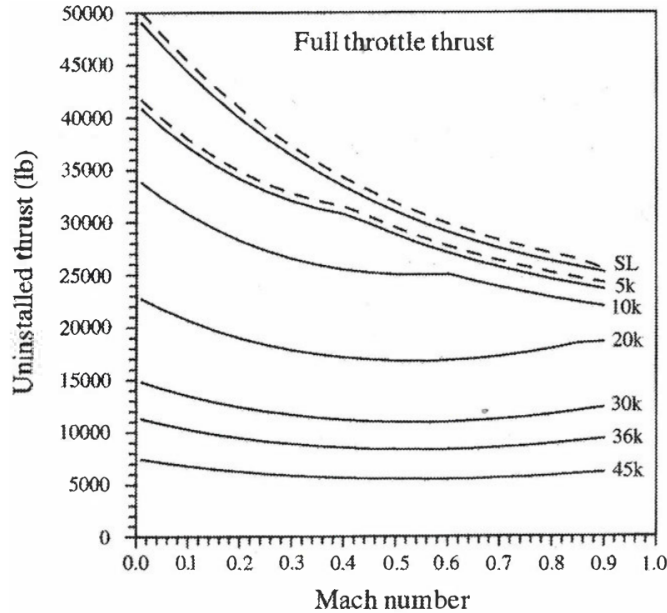


Figure 3.1: High-Bypass Turbofan characteristic curves as a function of flight altitude and Mach number

$$\left(\frac{T}{W_0}\right)_{\text{cruise}} = \left(\frac{T}{W}\right)_{\text{cruise}} \left(\frac{W_{\text{cruise}}}{W_{\text{takeoff}}}\right) \left(\frac{T_{\text{takeoff}}}{T_{\text{cruise}}}\right) = 0.0582 \cdot 0.955 \cdot 2.94 = 0.164 \quad (3.4)$$

3.2 Wing Loading

The wing loading analysis have been carried out for several mission segments, which are in order: takeoff, climb, cruise, loiter and landing. The smallest of them was chosen, in order to have the largest wing area and guarantee the success of all flight phases. For a right comparison between different performance, it is necessary to scale all wing loading to the initial of mission, using the segment weight fractions founded in the previous section. In this section we may also find other thrust-weight ratios that when scaled and compared with those already obtained allow us to make the final choice on this ratio.

3.2.1 Takeoff

For the preliminary calculation of wing loads, it was necessary to estimate the lift coefficient for maximum flap opening and for takeoff condition.

Maximum lift coefficient depends upon the wing geometry, airfoil shape, flap geometry and span, leading-edge slot or slat geometry, Reynolds number, surface texture and interference from other parts of aircraft. Most aircraft use different flap setting for takeoff and landing. During landing, the flaps will be deployed the maximum amount, however, for takeoff the maximum flap angle will probably cause more drag than desirable for rapid acceleration and climb. This fact was taken into account in the calculation of the first attempt $C_{L_{max}}$. In fact, we set the $C_{L_{max,TO}}$ be 80% of the $C_{L_{max,LND}}$.

For a better initial estimate of maximum lift, it is necessary to resort to test results and historical data. The available typical trends were used to determine the maximum lift coefficient as function of sweep angle $\Lambda_{\bar{c}/4}$ for various flap-slat configurations. In this first rough approximation, we chose not to differ much from the wing configuration of the reference aircraft, so from wing sweep historical trend, by choosing *Scorpion Mz M_{max}*, a sweep angle $\Lambda_{LE} = 30$ deg turned out, which results to $\Lambda_{\bar{c}/4} = 10$ deg. At this point, knowing $\Lambda_{\bar{c}/4}$ value,

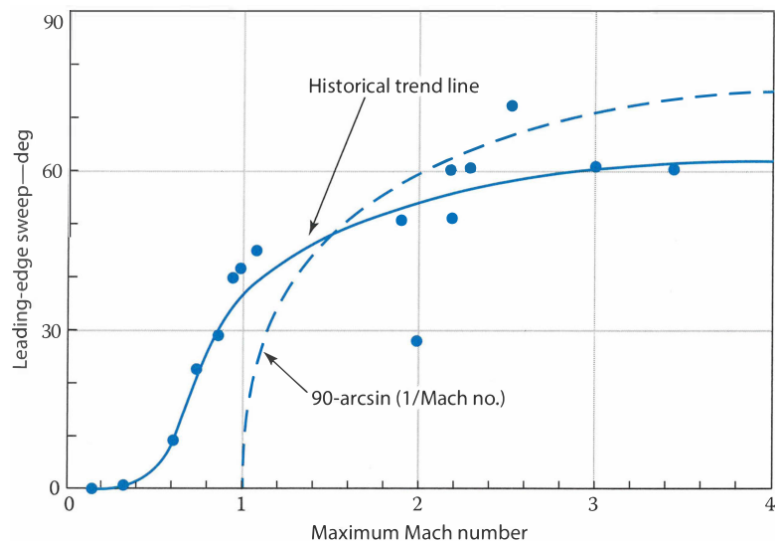


Figure 3.2: Wing sweep historical trend

and choosing a double slotted flap and slat configuration, $C_{L_{max}}$ can be derived. The reason for this choice in having to meet a strict take-off distance requirement, even when compared to other reference aircraft that have a less stringent requirement. Moreover, to date, most business jets, especially long range ones, adopt this configuration, which although complex and expensive, is very reliable and allows us to obtain optimum hypersostation.

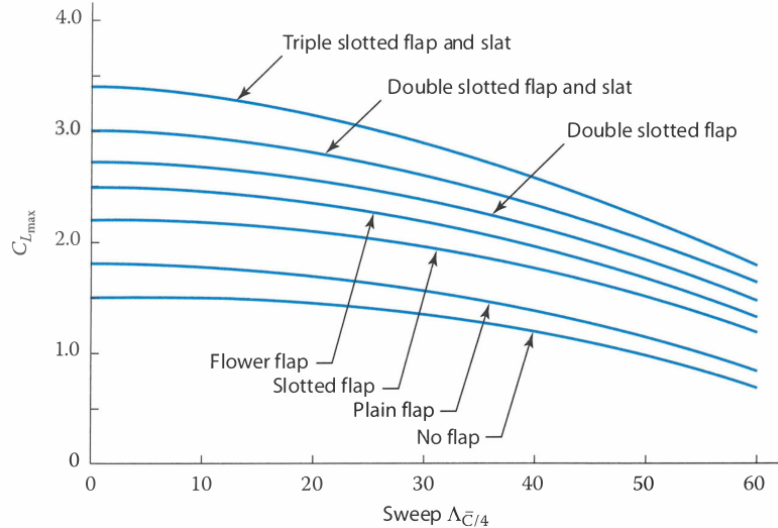


Figure 3.3: Maximum lift coefficient as a function of sweep angle

$$C_{L_{max}} = 2.9 \quad C_{L_{max,TO}} = 0.8 \cdot C_{L_{max}} = 2.32 \quad (3.5)$$

The approach proposed by Raymer was used to find a first-guess value for wing loading during take-off. This approach uses a parameter, the takeoff parameter (*TOP*) defined as shown in the 3.6, which is directly related to takeoff wing loading. The *TOP* at this stage is a known parameter from historical data, depending on the takeoff distance (remembering the imposed requirement of *TODR* = 4921 ft).

$$\text{TOP} = \frac{W/S}{\sigma C_{L_{TO}} T/W} = 240 \text{ lb/ft}^2 \Rightarrow \left(\frac{W}{S} \right)_{\text{TO, first guess}} \quad (3.6)$$

$$C_{L_{TO}} = \frac{C_{L_{max,TO}}}{1.1^2} = 1.92 \quad (3.7)$$

Where σ is the density ratio, at the altitude of the departure airport and $C_{L_{TO}}$ is the takeoff lift coefficient, not to be confused with the maximum. The MATLAB script realised allows the choice of the density value during the takeoff phase between two alternatives: at sea level in standard conditions or in extreme conditions at an altitude of 5000 ft in hot day. This last option, if chosen, will result in a sizing that ensure wider operation capabilities. At this point from the 3.6 the first rough value of W/S at takeoff is calculated, using the T/W first attempt value at takeoff found above.

Iterative scheme with flight mechanic approach

At this stage, having a first attempt value of W/S at takeoff, an iterative process was constructed, using the flight mechanics approach for takeoff. In this way, the W/S value was reduced with each iterative cycle, until the runway length requirement was met. Within the iterative scheme, the following quantities were calculated from the updated wing loading in each step. TODR was considered as the sum of 3 distances: obstacle clearance distance, maneuver distance and rolling distance. For the obstacle clearance distance, according to FAR regulations, the altitude of the obstacle (h_0) was considered equal to 35 ft (10.67 m), while the V_2 speed was set equal to $1.2V_{st}$. The stall speed, the curvature radius and the climb angle are expressed in 3.8, where $n_z = 1.2$.

$$V_{st} = \sqrt{\frac{2(W/S)_{TO}}{\rho_{SL} C_{L_{max,TO}}}} \quad R = \frac{V_2^2}{g(n_z - 1)} \quad \gamma = \arccos\left(1 - \frac{h_0}{R}\right) \quad (3.8)$$

$$d_h = R \sin(\gamma) \quad (3.9)$$

Considering a rotation time $\Delta_{tr} = 2$ s and a rotation speed $V_r = 1.2V_{st}$, the maneuver distance is:

$$d_m = \Delta_{tr} V_r \quad (3.10)$$

For last distance calculated, which is the first segment of the runway during the takeoff maneuver, the following equation was, like the others, iteratively solved:

$$\bar{a} = g \left[\frac{T}{W} - \mu - \frac{\rho_{SL} \left(\frac{V_R}{\sqrt{2}} \right)^2}{2(W/S)} (C_{D0} + K C_{L,opt}^2 - \mu C_{L,opt}) \right] \quad (3.11)$$

In which the aircraft's rolling resistance, μ , is determined by the type of runway surface, in the first instance, a value of $\mu = 0.02$ as in a dry runway was assumed. For a better estimate of C_{D0} the equivalent skin friction method was used, knowing the S_{wet}/S_{ref} ratio and considering a skin friction coefficient $C_{fe} = 0.003$ as suggested in literature for civil transport aircraft. In respect of this, it was found:

$$C_{D0} = C_{fe} \frac{S_{wet}}{S_{ref}} = 0.0183$$

Finally, the last remaining unknown term is $C_{L,opt}$ which is described by the following relationship:

$$C_{L,opt} = \frac{\mu}{2K}$$

At this point, the rolling distance can be found within the loop as reported in 3.12 and also the TODR as sum of d_r , d_m and d_h . At each iteration, the result obtained will then be compared with the requirement until convergence is achieved.

$$d_r = \frac{V_r^2}{2\bar{a}} \quad \text{TODR} = d_r + d_m + d_h \quad (3.12)$$

The main results obtained are shown in table 3.1, considering the airport condition at sea level in standard day and considering also the wing loading associated to the departure in the worst operating condition, from the airport located at 5000 feet in hot day.

Parameter	Symbol	Value (BE)	Value (SI)
Stall speed	V_{st}	115 kn	213 km/h
Mach stall	M_{st}	0.174	0.174
Mach during roll phase	M_{roll}	0.21	0.21
TODR requirement	$TODR_{req}$	satisfied	satisfied
Standard condition takeoff wing loading	$(W/S)_{TO}$	104 lb/ft ²	4980 N/m ²
Worst condition takeoff wing loading	$(W/S)_{TO}$	82.34 lb/ft ²	3942.5 N/m ²

Table 3.1: Takeoff wing loading main results

3.2.2 Climb

As far as the climb phase is concerned, several assumptions must be made regarding certain necessary data that are not available. These data are the climb speed and maximum climb rate and were obtained considering a typical mission profile of the reference aircraft. The values are the following:

$$V_{cl} = 250 \text{ kn (129 m/s)} \quad RoC_{max} = 3100 \text{ ft/min (15.8 m/s)}$$

These quantities are derived from an average of the values recorded for a typical G650ER climb profile. It should be noted that the climb is actually divided into climb portions at different speeds and ROCs. Instead, in the following discussion, the climb has been considered as a single segment and the results presented refer to the standard runway starting condition (those considering the worst condition can be found in the MATLAB script, but from here on only the classic mission will be considered). Some useful data can be found in the following table. Knowing all these parameters, the T/W ratio for the climb phase can be determined:

Parameter	Symbol	Value (BE)	Value (SI)	Evaluation method
Climb gradient	G	0.1224	0.1224	$G = RoC_{max}/V_{cl}$
Service ceiling	h_{ceil}	46000 ft	14000 m	$h_{ceil} = h_{cr} + 10000 \text{ ft}$
Climb density	ρ_{cl}	0.0004386 slg/ft ³	0.226 kg/m ³	$\rho_{cl} = (\rho_{SL} + \rho_{ceil})/2$
Climb altitude	h_{cl}	23000 ft	7000 m	$h_{cl} = (h_{SL} + h_{ceil})/2$
Climb Mach	M_{cl}	0.5449	0.5449	$M_{cl} = \frac{V_{cl}}{\sqrt{\gamma R(T_{SL} \cdot 0.0065 h_{cl})}}$
Climb dynamic pressure	Q	200 lb/ft ²	976 kg/m ³	$Q = 1/2 \cdot \rho_{cl} V_{cl}^2$
Parasite drag coefficient	$C_{D0_{cl}}$	0.0383	0.0383	$C_{D0_{cl}} = C_{D0} + 0.02$
Oswald factor	e_{cl}	0.76	0.76	$e_{cl} = 0.95e$
Induced drag factor	K_{cl}	0.0419	0.0419	$K_{cl} = 1/(\pi A Re_{cl})$
Max. Efficiency climb	$E_{max_{cl}}$	12.484	12.484	$E_{max_{cl}} = \frac{1}{2\sqrt{C_{D0_{cl}} K_{cl}}}$

$$\left(\frac{T}{W}\right)_{cl} = G + \frac{1}{E_{max_{cl}}} \quad (3.13)$$

$$\left(\frac{W}{S}\right)_{cl} = \frac{Q((T/W)_{cl} - G)}{2K_{cl}} \left(1 + \sqrt{1 - \frac{1}{(E_{max_{cl}})^2((T/W)_{cl} - G)^2}}\right) \quad (3.14)$$

Obviously, these values should be scaled with respect to the take-off conditions, according to the following procedure, where the thrust lapse rate was found in similarly way to section 3.1, considering the figure 3.1:

$$\left(\frac{T}{W_0}\right)_{cl} = \left(\frac{T}{W}\right)_{cl} \left(\frac{W_1}{W_0}\right) \left(\frac{T_{takeoff}}{T_{climb}}\right) = 0.368 \quad (3.15)$$

$$\left(\frac{W_0}{S}\right)_{cl} = \frac{(W/S)_{cl}}{W_1/W_0} = 123.6 \text{ lb/ft}^2 \quad (3.16)$$

All that remains is to determine the climb gradient under the conditions of an inoperative engine (G_{OEI}), defined as:

$$G_{OEI} = \left(\frac{T}{W}\right)_{cl} - \frac{1}{E_{max_{cl}}} = 0.0212 \quad (3.17)$$

where a halving of the thrust-to-weight ratio was assumed, corresponding to the failure of an engine. This value is to be compared with the minimum climb gradient in the case of O.E.I. according to FAR25, which is 0.012. The requirement is therefore met.

3.2.3 Cruise

For the cruise phase, the wing load calculation is based on the following equation:

$$\left(\frac{W}{S}\right)_{cr} = \frac{1}{2} \cdot \rho_{cr} V_{cr}^2 \sqrt{\pi A Re C_{D0}/3} \quad (3.18)$$

where the still unspecified parameters are given below:

$$\rho_{cr} = 0.0007087 \text{ slug/ft}^3 \quad V_{cr} = 774.7 \text{ ft/s}$$

The value obtained should be scaled with respect to the takeoff conditions, obtaining:

$$\left(\frac{W_0}{S}\right)_{cr} = \frac{(W/S)_{cr}}{\left(\frac{W_2}{W_1} \frac{W_1}{W_0}\right)} = 87.15 \text{ lb/ft}^2 \quad (3.19)$$

In addition to the wing loading relative to cruising speed, the wing loading relative to maximum speed conditions was also calculated, obtaining:

$$V_{max} = 871.54 \text{ ft/s} \quad \left(\frac{W}{S}\right)_{V,max} = \frac{1}{2} \cdot \rho_{cr} V_{max}^2 \sqrt{\pi A Re C_{D0}/3}$$

$$\left(\frac{W_0}{S}\right)_{V,max} = \frac{(W/S)_{V,max}}{\left(\frac{W_2}{W_1} \frac{W_1}{W_0}\right)} = 110.3 \text{ lb/ft}^2 \quad (3.20)$$

3.2.4 Loiter

For the loiter phase, a loiter speed was assumed, based on a range of indicative values suggested by Raymer:

$$V_{loit} = 200 \text{ kn} (= 337.6 \text{ ft/s})$$

The expression used to calculate the wing loading is as follows

$$\left(\frac{W}{S}\right)_{loit} = \frac{1}{2} \cdot \rho_{loit} V_{loit}^2 C_{L_{be}} \quad (3.21)$$

in which the density at a loiter altitude of 10000 ft was inserted and the dynamic pressure and C_L of best endurance, calculated as follows:

$$\rho_{loit} = 0.00175549 \text{ slug/ft}^3 \quad C_{L_{be}} = \sqrt{C_{D0}/K} = 0.6782$$

Finally, the result was scaled with respect to the takeoff conditions using the usual procedure:

$$\left(\frac{W_0}{S}\right)_{loit} = \frac{(W/S)_{loit}}{\left(\frac{W_3}{W_2} \frac{W_2}{W_1} \frac{W_1}{W_0}\right)} = 109.42 \text{ lb/ft}^2 \quad (3.22)$$

3.2.5 Landing

For the landing phase, first a preliminary estimate of the wing loading, based on Raymer's approach, was used following the approach used for the takeoff phase.

$$\left(\frac{W}{S}\right)_{lnd} = \frac{s_{lnd} - s_a}{80 \cdot \sigma C_{L_{max}}} \quad (3.23)$$

where s_a is set equal to 1000 ft, as suggested by the textbook for the class of aircraft considered, $C_{L_{max}}$ was considered equal to 2.9, and $s_{landing}$ was set equal to $TODR_{req}$. Discussion about $C_{L_{max}}$ value has already been made in the takeoff section. From this preliminary estimate, a first-attempt value for the stall speed in landing phase of the aircraft could also be determined:

$$V_{st_{lnd}} = \sqrt{\frac{2(W/S)_{lnd}}{\rho_{SL} C_{L_{max}}}}$$

However, it was judged appropriate to combine this approach with the classical flight mechanics approach for a more accurate calculation of runway length at landing. As is well known, the runway length at landing consists of three lengths: those of approach, touch down and brake.

The approach length can be estimated as follows:

$$d_a = E_{lnd} \left(h_0 + \frac{V_3^2 - V_{td}^2}{2g} \right) \quad (3.24)$$

Where all necessary values were calculated as follows: $h_0 = 50$ ft which is the obstacle clearance height, specified by FAR25, $V_3 = 1.3 \cdot V_{st_{lnd}}$ and $V_{td} = 1.15 \cdot V_{st_{lnd}}$ which are the approach and touch down speed, respectively.

The aerodynamic data are also recalculated for the specific flight condition, considering a deterioration in drag due to the presence of the undercarriage and of the Oswald factor due to the deflection of the flaps ruining the lift distribution.

$$e_{lnd} = 0.9e \quad C_{D0_{lnd}} = C_{fe} \frac{S_{wet}}{S_{ref}} + 0.002 + 0.007 \quad E_{lnd} = \frac{C_{L_{max}}}{C_{D0_{lnd}} + K_{lnd} \cdot C_{L_{max}}^2}$$

The friction factor from FAR regulations $\mu = 0.4$ is used and thus the Drag-to-Weight ratio was found.

$$\left(\frac{D}{W} \right) = \frac{\rho_{SL} (V_{td}/\sqrt{2})^2 C_{D_{lnd}}}{2(W/S)_{lnd}}$$

Having defined a $t_{transition}$ equal to 1.5 s, the touch down distance was calculated as follows:

$$d_{td} = t_{tr} V_{td} \quad (3.25)$$

After that, the brake distance was calculated, where the average acceleration was estimated in 3.26.

$$d_{br} = \frac{V_{td}^2}{2|a_{mean}|} \quad a_{mean} = g \cdot \left(-\frac{D}{W} - \mu \right) \quad (3.26)$$

For commercial aircraft, FAR 25 provides a safety margin of 1.67 to be multiplied to the sum of all the distances calculated.

$$d_{tot_{lnd}} = 1.67(d_a + d_{td} + d_{br}) \quad (3.27)$$

The results are intentionally not reported, because after this first estimate was finished, it was necessary to correct the first-attempt wing loading by means of a while loop implemented as follows:

- the loop condition is based on satisfying the landing distance requirement, which must be less than or at most equal to the $TODR$;
- the cyclic operations involve a reduction of the wing loading, from which it is necessary to recalculate all the quantities required to estimate the d_{tot} (stall speed, V_3 , V_{td} , D/W , a_{mean} and hence d_a , d_{td} , d_{br} and d_{tot})

The final results are:

$$V_{st_{lnd}} = 104.74 \text{ kn} (= 53.9 \text{ m/s}) \quad \left(\frac{W_0}{S} \right)_{lnd} = \frac{(W/S)_{lnd}}{\left(\frac{W_5}{W_4} \frac{W_4}{W_3} \frac{W_3}{W_2} \frac{W_2}{W_1} \frac{W_1}{W_0} \right)} = 175 \text{ lb/ft}^2 \quad (3.28)$$

3.3 Wing loading and Thrust-to-Weight selection

The final selection of W/S and T/W is based on the following criteria:

- the final wing loading must be the lesser of those calculated for each flight phase, in order to ensure an adequate wing area to meet the requirements expressed for each phase;
- the final thrust-to-weight ratio must be the greater of those calculated, in order to ensure sufficient thrust for flight operations.

In conclusion, the final values of the two ratios are:

$$\left(\frac{W}{S} \right) = 87.15 \text{ lb/ft}^2 \quad \left(\frac{T}{W} \right) = 0.368 \quad (3.29)$$

By examining the values obtained and comparing them with those of the reference aircraft, it can be seen that the results obtained are reasonable estimates.

Chapter 4

Initial Sizing and Design Layout

4.1 Refined sizing

In the previous chapters, a quick method based upon minimal information about the design was used to estimate the sizing parameters. At this point in the project, refined sizing can be carried out.

The equation used for the calculus of the refined takeoff gross weight is the 4.1, obviously also in this case the solution is found iteratively within a loop.

$$W_0 = W_{\text{crew}} + W_{\text{payload}} + W_{\text{fuel}} + \left(\frac{W_e}{W_0} \right) W_0 \quad (4.1)$$

The crew and the payload weights were the same as the previous calculated values, thus, they were respectively considered equal to 720 lb and 4050 lb. The empty weight fraction was estimated using the following improved statistical equation:

$$\frac{W_e}{W_0} = 0.32 + 0.66 W_0^{-0.13} AR^{0.3} \left(\frac{T}{W} \right)^{0.06} \left(\frac{W}{S} \right)^{-0.05} M_{\max}^{0.05} = 0.54 \quad (4.2)$$

The fuel weight was calculated by the following method:

$$W_{\text{fuel}} = 1.06 \sum_{i=1}^{11} \left(1 - \frac{W_{i+1}}{W_i} \right) W_i = 45917 \text{ lb} \quad (4.3)$$

The values of each weight fraction were found as already done in the first attempt sizing. For the cruise and loiter segment (calculated with the Breguet equations), a more accurate estimation of L/D was used, by expressing the efficiency as the inverse of the drag divided by the weight. Where the wing loading and subsequent weight fraction are those evaluated at the condition being evaluated.

$$\frac{L}{D} = \frac{1}{\frac{qC_{D0}}{W/S} + \frac{W}{S} \frac{1}{q\pi A Re}} \quad (4.4)$$

Another significant change in calculus method was done with the estimation of the climb fuel fraction. This time, Mach speed during the beginning and the end of the climb phases was involved by solving 4.5 using in this way the average Mach number in climb phases.

$$\frac{W_i}{W_{i-1}} = 1.0065 - 0.0325M \quad (4.5)$$

Finally, solving the eq. 4.1 by iteration, the value of the new takeoff gross weight was obtained

Segment	Weight fraction	Value
Warmup, taxi, takeoff	W_1/W_0	0.970
Climb	W_2/W_1	0.986
Cruise	W_3/W_2	0.65
Descent	W_4/W_3	0.993
Loiter	W_5/W_4	0.993
Aborted landing	W_6/W_5	0.995
Climb	W_7/W_6	0.986
Cruise to AAP	W_8/W_7	0.977
Descent	W_9/W_8	0.993
Loiter	W_{10}/W_9	0.993
Landing at AAP	W_{11}/W_{10}	0.995

Table 4.1: Refined mission segment weight fraction

and with it, also the required thrust and the new wing surface, as reported in table below: At

Parameter	Symbol	Value (BE)	Value (SI)
MTOW	W_0	105767 lb	47975 kg
Empty weight	W_e	57153 lb	25924 kg
Fuel weight	W_f	45917 lb	20827 kg
Volume of fuel tanks req.	V_{fuel}	918 ft ³	26 m ³
Payload weight	W_{pl}	4050 lb	1840 kg
Crew weight	W_{cr}	720 lb	330 kg
Wing Loading	W/S	87.15 lb/ft ²	4173 N/m ²
Thrust-to-Weight ratio	T/W	0.37	0.37
Engines req. thrust	T_{req}	38963 lb	173 kN
Wing area	S_{ref}	1213.7 ft ²	112.7 m ²

Table 4.2: Main results of refined sizing

this stage of the project, it is possible to begin to appreciate the goodness of the preliminary calculations by making a quick comparison of the significant results with the reference aircraft as shown in the table 4.3.

4.2 Fuselage

A fairly quick way of estimating the overall dimensions of the fuselage is based on the maximum take-off weight of the aircraft and the fineness ratio (φ) as expressed in 4.6, which is

Parameter	G650-ER	Scorpion MZ
S_{wet}/S_{ref}	6.1	6.1
MTOW (lb)	103600	105767
W_{empty} (lb)	53630	57153
$W_{empty}/MTOW$	0.52	0.54
W_{fuel} (lb)	48200	45917
V_{stall} (kn)	110	115
TODR (ft)	6300	4921
M_{cr}	0.85	0.8
R (nmi)	7000	6500 + 350
W/S (lb/ft ²)	81	87.15
T/W	0.38	0.37
AR	9.95	10
S_{ref} (ft ²)	1284	1214
T_{req} (lb)	38850	38963

Table 4.3: Gulfstream G650ER vs Scorpion MZ Aircraft comparison of main parameters

the ratio of fuselage length to maximum diameter, considering of course an equivalent diameter. Numerous design books indicate that drag is minimized with a fineness ratio of around three. This is an odd conclusion because few successful designs actually use such a low fineness ratio, in particular for subsonic aircraft today, the ratio often assumes values of 6 to 10, and for supersonic aircraft it can be as high as 14. A first attempt value chosen for our business jet was $\varphi = 10$. Once equation 4.6 was solved, the results obtained with this fineness ratio were critically observed, because it is good to note that when making the actual design layout, the various real-world constraints such as cockpit and payload shape must take priority. For most design efforts, in fact, the realities of packaging the internal components will ultimately establish the fuselage length and diameter-but it is good to know the optimal fineness ratio as a layout goal.

As far as seats are concerned, there are no particular limits to be observed for this type of aircraft. For this reason, it was decided to use seat sizes typically used in first class. The length, width and height of the seats are respectively: 1.45 ft, 1.48 ft, 3.3 ft. In addition, several relax areas were provided in which sofas were placed. The seating arrangements were made with safety in mind, with a total of 18 seats for passengers, two for crew members and the cockpit for the two pilots. Finally, the rear area of the fuselage was intentionally left empty to allow for the positioning of the toilet and baggage area.

Parameters A and C were selected for our aircraft class as $A = 0.67$ and $C = 0.43$.

$$L_{fus} = AW_0^C = 96.9 \text{ ft} (\approx 29.5 \text{ m}) \quad D_{fus} = \frac{1}{\varphi} \cdot L_{fus} = 9.7 \text{ ft} (\approx 3 \text{ m}) \quad (4.6)$$

During concept layout, the designer must consider the requirements for aerodynamics based upon experience, understanding, and a "good eye". The overall configuration arrangement and "cleanliness" of an aircraft has a major effect upon aerodynamic efficiency. Good lofting

produces good aerodynamics. Slope discontinuities (breaks) in the longitudinal direction are very bad. If there needs to be a longitudinal break, it should be smoothed following a radius roughly equal to the fuselage diameter.

In general, aft-fuselage upsweep should be minimized as much as possible, especially for high-speed aircraft. An upsweep of about 25 deg can be tolerated for a rear-loading transport aircraft provided that the fuselage lower corners are fairly sharp. This causes a vortex flow pattern that reduces the drag penalty. This consideration was taken into account when the final sketch was made.

4.3 Wing

The actual wing size can now be determined simply as the takeoff gross weight divided by the takeoff wing loading. This is the reference area of the trapezoidal wing and includes the area extending into the aircraft centerline, its value has already been found and reported in section 4.1. The span can be derived by inverting the definition of the aspect ratio, which is also known.

$$S_{ref} = \frac{W_0}{(W/S)} = 1213.7 \text{ ft}^2 \quad b = \sqrt{AR \cdot S_{ref}} = 110.2 \text{ ft}$$

Sweeping the wing backward diverts air towards the wing tips due to the wing's shape and pressure distribution. This leads to increased lift towards the tips compared to an unswept wing. To achieve the desired elliptical lift distribution, increased tapering is necessary. While wing sweep increases weight, reduces lift, and affects the performance of ailerons and flaps, it is commonly used in high-speed aircraft due to its advantages. Wing sweep mitigates the adverse effects of transonic and supersonic flow. Shock formation on a swept wing at high subsonic speeds is determined by the air velocity roughly perpendicular to the leading edge, which appears slower due to the shorter distance from leading edge to trailing edge. This prevents shock formation. For high-speed flight, a swept wing is preferred, while for cruise, takeoff, and landing, an unswept wing is more desirable. A sweep angle at the leading edge of 30 deg was chosen from the plot 3.2 as mentioned previously. The wing sweep and aspect ratio together have a strong effect on the wing-alone pitch-up characteristics. "Pitch-up" is the undesirable tendency of some aircraft, upon reaching an angle of attack near stall, to suddenly and uncontrollably increase the angle of attack. Figure 4.1 describes boundaries for pitch-up avoidance for combinations of wing quarter-chord sweep angle and aspect ratio. A wing sweep at the quarter of chord of 10 deg was used following this treatment as mentioned in previously section. The exact wing sweep required to avoid shocks depends upon the selected airfoil, thickness ratio, taper ratio, and of course, the desired flight Mach number. Because wing weight increases with wing sweep, a tradeoff is always involved.

Taper ratio (λ) is the ratio of the tip chord to the centerline root chord of a wing. Taper affects the lift distribution along the wing span. An untapered wing has excessive chord length toward the tip compared to an ideal elliptical wing, causing it to generate more lift towards the tip than desired. This results in higher drag compared to an elliptical wing with the same

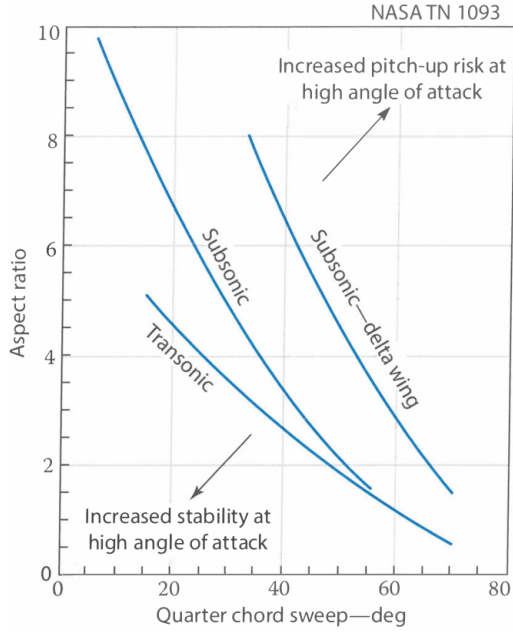


Figure 4.1: Tail off pitch-up boundaries

aspect ratio (about 7% more). Tapering the wing by reducing the tip chords helps alleviate this issue. The desired taper ratio required to approximate the elliptical lift distribution for a swept wing can be taken from the following plot. A taper ratio of $\lambda = 0.3$ was chosen.

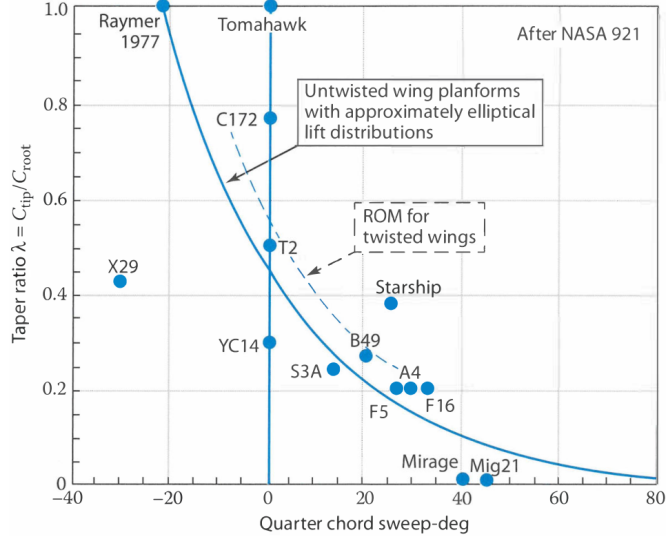


Figure 4.2: Effect of sweep on desired taper ratio

Wing twist is used to prevent tip stall and to revise the lift distribution to approximate an ellipse. For initial design purposes, historical data should be used. Typically, 3 deg of twist provides adequate stall characteristics.

Wing dihedral refers to the angle of the wing relative to the horizontal when viewed from the front. It has the tendency to level the aircraft when it is banked. This is achieved by introducing a rolling moment due to the sideslip caused by the bank angle. The aircraft slides

towards the lowered wing, increasing its angle of attack, which generates a rolling moment proportional to the dihedral angle.

In the case of an aft-swept wing, a negative rolling moment is produced, which is proportional to the sine of twice the sweep angle. This effectively adds to the geometric dihedral of the wing. The position of the wing on the fuselage also affects the effective dihedral. When the fuselage experiences sideslip, it pushes air over and under itself. If the wing is mounted high, the air pushed over the top of the fuselage imparts an increased dihedral effect on the forward wing. The opposite is true for a low-mounted wing.

Excessive dihedral effect can lead to "Dutch roll," which is a repeated side-to-side motion involving yaw and roll.

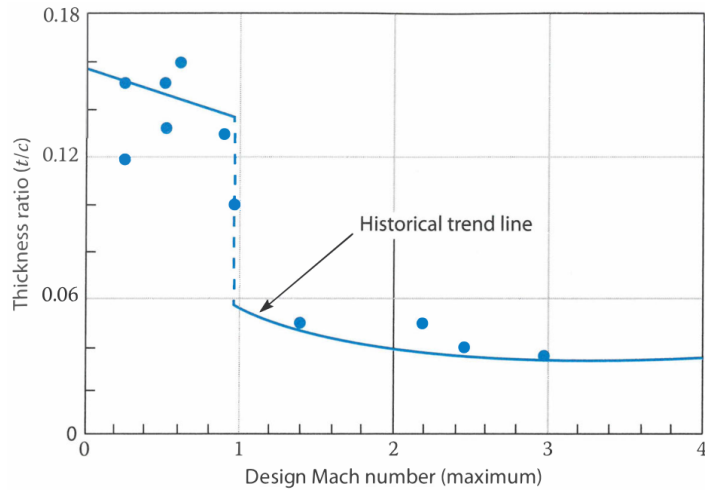
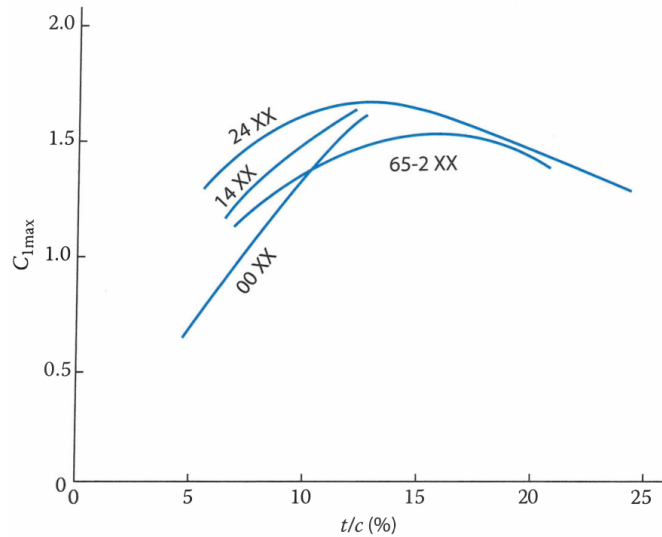
Selecting the appropriate dihedral angle is a complex task as it involves considering all these effects. Currently, there is no simple technique for determining the dihedral angle, and it often requires estimation based on historical data followed by analysis and revision during the design process. In respect of this, following the values recommended by Raymer, a dihedral of 3 deg was selected, due to the wing vertical position, which was set to low for the reasons that are about to be explained below.

It is clear that an aircraft carrying people in the fuselage cannot be equipped with a mid-wing. With regard to the high-wing, which is characterised by various pros and cons, it was noted that the vast majority of business jets are equipped with a low wing, which is why the focus was on examining the advantages of this choice. A low-wing aircraft design offers several advantages. The gear trunnion can be directly attached to the strong wing box, requiring minimal reinforcement. The retracted gear can be stored within the wing, wing-fuselage fairing, or nacelle, eliminating the need for an external blister. For adequate engine clearance, the fuselage is positioned higher off the ground compared to high-wing aircraft. This increases landing-gear weight but provides greater ground clearance, reducing the upsweep of the aft-fuselage and lowering drag.

The airfoil is the heart of the airplane and it affects the cruise speed, takeoff and landing distances, stall speed, handling qualities (especially near the stall), and overall aerodynamic efficiency during all phases of flight.

The "airfoil thickness ratio" (t/c) refers to the maximum thickness of the airfoil divided by its chord. Airfoil thickness ratio has a direct effect on drag, maximum lift, stall characteristics, and structural weight. For initial selection of the thickness ratio, the historical trend shown in figure 4.3 can be used. The plot 4.4 on effect of t/c on maximum lift can be used to select a family of airfoil. Therefore, the NACA 2414 airfoil was chosen for the wing of the aircraft under design.

Having defined the different parameters analysed, it was possible to calculate the root, tip and mean aerodynamic chord and its spanwise location. All wing parameters obtained are given in the table 4.4 At this point, a check must be made concerning the actual availability of useful volume within the wing for the placement of fuel tanks. The volume tank required after the refined weight sizing was 918 ft^3 . Therefore, it is necessary to estimate the portion of volume available within the wing. To do this, an average thickness of the wing was considered,

**Figure 4.3:** Thickness ratio historical trend**Figure 4.4:** Effect of t/c on maximum lift

Parameter	Symbol	Value (BE)	Value (SI)
Wing reference surface	S_{ref}	1213.7 ft ²	112.76 m ²
Wing span	b	110.2 ft	33.6 m
Aspect Ratio	AR	10	10
Root wing chord	c_{root}	16.95 ft	5.17 m
Tip wing chord	c_{tip}	5.08 ft	1.55 m
Mean wing chord	c_{mean}	12.08 ft	3.68 m
Spanwise location MAC	\bar{Y}	22.6 ft	6.89 m
Taper ratio	λ	0.3	0.3
Thickness ratio	t/c	0.14	0.14
Sweep at quarter chord	$\Lambda_{c/4}$	10 deg	10 deg
Airfoil	$NACA$	2414	2414

Table 4.4: Wing parameters

expressed as the product of average chord and t/c ratio, results $t_{mean} = 1.69$ ft.

Then, a portion of the wing surface equal to half of a half-wing, that is, a quarter of the total surface area, was considered. Calculating the tank volume by multiplying this portion by the average thickness and multiplying the obtained value by two, considering that the tanks are present in both wings, we obtain an estimate of the actual available tank volume which meets the space requirement.

$$V_{wingav} = 1026 \text{ ft}^3 > 918 \text{ ft}^3$$

4.4 Horizontal and Vertical Tail

Tails provide for trim, stability, and control:

- for the horizontal tail, trim primarily involves balancing of the moment created by the wing, while for the vertical tail of multi-engine aircraft must be capable of providing sufficient trim in the event of an engine failure;
- tail is a key element of stability, acting much like the fins on an arrow to restore the aircraft from an upset in pitch or yaw;
- tail must be sized to provide adequate control power at all critical conditions (that for the horizontal tail include nosewheel liftoff, low-speed flight with flaps down, and transonic maneuvering; for the vertical tail, they include engine-out flight at low speeds, maximum roll rate, and spin recovery). Control power depends upon the size and type of the movable surface as well as the overall size of the tail itself.

The "T-tail" arrangement is widely used for business jets. Although it is usually heavier than a conventional tail because the vertical tail must be strengthened to support the horizontal one, the T-tail provides compensating advantages in many cases:

- because of end-plate effect, it allows a smaller vertical tail;
- it lifts the horizontal tail clear of the wing wake and propwash, which makes it more efficient and hence allows reducing its size;
- it reduces buffet on the horizontal tail, which reduces fatigue for both the structure and the pilot;
- it allows the use of engines mounted in pods on the aft fuselage;
- it is considered stylish, which is not a so trivial consideration for a business jet!

A T-tail requires a wing designed to avoid pitch-up without a horizontal tail, as described by fig. 4.1. Some geometric parameters for the tails can be selected. Tables 4.6 and 4.5 provide selected values of tail aspect ratio and taper ratio, taken by Raymer's suggestions and CAD validation considering a 3D model of the reference aircraft. T-tail aircraft have lower vertical tail aspect ratios to reduce the weight penalty of the horizontal tail's location on top of the

vertical tail.

Leading-edge sweep of the horizontal tail is usually set to about 5 deg more than the wing sweep. This tends to make the tail stall after the wing and provides the tail with a higher critical Mach number than the wing. This avoids loss of elevator effectiveness due to shock formation. Vertical-tail sweep varies between about 35 and 55 deg. For a high-speed aircraft, vertical-tail sweep is used primarily to ensure that the tail's critical Mach number is higher than the wing.

Tail thickness ratio is usually similar to the wing thickness ratio, as determined by the historical guidelines provided in the wing-geometry section. For a high-speed aircraft, the horizontal tail is frequently about 10% thinner than the wing to ensure that the tail has a higher critical Mach number.

For conceptual design, it is usually acceptable simply to draw tail surfaces that "look right", based upon prior experience and similar designs, provided that the total area is correct. The surface areas required for tail are directly proportional to the aircraft's wing area. An initial estimation was made using the "tail volume coefficient" method. The force due to tail lift is proportional to the tail area. Thus, the tail effectiveness is proportional to the tail area times the tail moment arm. This product has units of volume, which leads to the "tail volume coefficient" method for initial estimation of tail size. Rendering this parameter nondimensional requires dividing by some quantity with units of length:

- For a vertical tail, the wing yawing moments that must be countered are most directly related to the wing span b_w . This leads to the "vertical tail volume coefficient"

$$c_{VT} = \frac{L_{VT}S_{VT}}{b_w S_w}$$

- For a horizontal tail or canard, the pitching moments that must be countered are most directly related to the wing mean chord C_w . This leads to the "horizontal tail volume coefficient"

$$c_{HT} = \frac{L_{HT}S_{HT}}{C_w S_w}$$

The moment arm L is approximated as the distance from the tail quarter-chord to the wing quarter-chord. The definition of tail moment arm is shown in fig.4.5. To calculate tail size, the moment arm must be estimated. This can be approximated at this stage of design by a percent of the fuselage length as estimated earlier. For aft-mounted engines the tail arm is about 45-50% of the fuselage length, so a L_{ht} equal to 50% of the fuselage length was chosen. Typical values for volume coefficients for Jet transport aircraft are $c_{HT} = 1$ and $c_{VT} = 0.09$. For a "T-tail," the vertical-tail volume coefficient can be reduced by approximately 5% due to the end-plate effect, and the horizontal tail volume coefficient can be reduced by about 5% due to the clean air seen by the horizontal. These values were used to calculate tail area.

$$S_{VT} = \frac{c_{VT}b_w S_w}{L_{VT}} = 235.8 \text{ ft}^2 \quad S_{HT} = \frac{c_{HT}\bar{C}_w S_w}{L_{HT}} = 287.4 \text{ ft}^2 \quad (4.7)$$

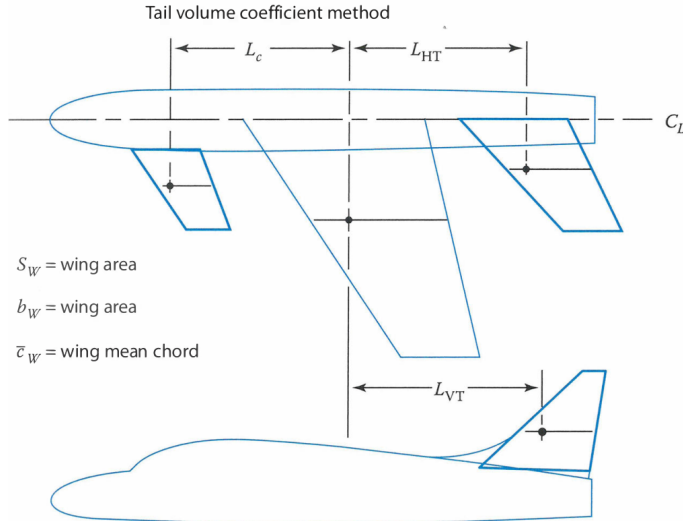


Figure 4.5: Initial tail sizing

The other geometric parameters of the vertical tail and the horizontal tail (span, root chord, tip chord, mean aerodynamic chord and its spanwise location) were derived from the same equations used for the wing. In the following tables, the results for the vertical tail and the horizontal tail are summarised.

Parameter	Symbol	Value (BE)	Value (SI)
Volume coefficient	c_{HT}	0.95	0.95
Tail arm	L_{HT}	48.5 ft	14.8 m
Area	S_{HT}	287.4 ft ²	26.7 m ²
Aspect Ratio	AR_{HT}	4.5	4.5
Taper Ratio	λ_{HT}	0.47	0.47
Span	b_{HT}	35.96 ft	10.96 m
Sweep angle at LE	$\Lambda_{LE_{HT}}$	33 deg	33 deg
Root chord	$c_{root_{HT}}$	10.87 ft	3.31 m
Tip chord	$c_{tip_{HT}}$	5.11 ft	1.56 m
Mean aerod. chord	$c_{mean_{HT}}$	8.34 ft	2.54 m
Spanwise location of MAC	Y_{HT}	7.91 ft	2.41 m
Thickness Ratio	$(t/c)_{HT}$	0.12	0.12
Airfoil	NACA	2412	2412

Table 4.5: Horizontal tail parameters

4.5 Engine and Nacelle

Aircraft sizing involves using either an existing fixed-size engine or designing a new rubber engine. A fixed-size engine has a predetermined size and thrust, while a rubber engine can be adjusted to any required size and thrust. The rubber engine can be scaled during the sizing process to maintain the desired thrust-to-weight ratio as the aircraft weight varies, enabling the aircraft to meet both performance and range goals. In contrast, a fixed-size engine limits

Parameter	Symbol	Value (BE)	Value (SI)
Volume coefficient	c_{VT}	0.0855	0.0855
Tail arm	L_{VT}	48.5 ft	14.8 m
Area	S_{VT}	235.8 ft ²	21.9 m ²
Aspect Ratio	AR_{VT}	1.1	1.1
Taper Ratio	λ_{VT}	0.7	0.7
Span	b_{VT}	16.11 ft	4.9 m
Sweep angle at LE	$\Lambda_{LE_{VT}}$	40 deg	40 deg
Root chord	$c_{root_{VT}}$	17.23 ft	5.25 m
Tip chord	$c_{tip_{VT}}$	12.06 ft	3.68 m
Mean aerod. chord	$c_{mean_{VT}}$	14.8 ft	4.51 m
Spanwise location of MAC	\bar{Y}_{VT}	7.91 ft	2.41 m
Thickness Ratio	$(t/c)_{HT}$	0.12	0.12
Airfoil	$NACA$	0012	0012

Table 4.6: Vertical tail parameters

the ability to simultaneously meet range and performance requirements. Developing a new engine is expensive, so most aircraft projects rely on existing engines. However, even when using an existing engine, designers may conduct rubber-engine design studies to determine the desired characteristics before making a final selection. This approach allows for exploration of engine options before committing to a specific engine choice.

When designing an aircraft with an existing engine, dimensions are obtained from the manufacturer. However, if a "rubber" engine is used, dimensions must be scaled from a nominal size to achieve the desired thrust. Designers can obtain estimated data from engine companies for hypothetical rubber engines, and sometimes engine companies provide computer programs that generate performance and dimensional data based on input parameters. Another method involves scaling an existing engine while assuming improvements due to advanced technologies. The dimensions that need to be scaled include length, diameter, and weight. The accessory package, including fuel pumps and control boxes, is located beneath the engine. If no suitable options are available, a parametric statistical approach can be used to define the nominal engine.

Therefore, after obtaining the nominal thrust of the reference aircraft engine and the thrust required by the design aircraft, a scaling factor was defined equal to the ratio of the required thrust to the nominal thrust.

$$SF = \frac{T_{req}}{T_{nom}} = 1.146 \quad (4.8)$$

Then, starting from the nominal dimensions (length and diameter) and weight of the reference engine, statistical formulas were used to derive the values for the rubber engine:

$$L_{nom} = 10.82 \text{ ft} \quad D_{nom} = 3.12 \text{ ft} \quad W_{nom} = 3605 \text{ lb}$$

$$L_{eng} = L_{nom} SF^{0.4} = 11.4 \text{ ft} \quad D_{eng} = D_{nom} SF^{0.5} = 3.34 \text{ ft} \quad W_{eng} = W_{nom} SF^{1.1} = 4188 \text{ lb} \quad (4.9)$$

With regard to the size of the nacelles, reference was made to statistical formulae proposed by Kundu [3]:

$$D_{nacelle} = 1.3D_{eng} = 4.34 \text{ ft} \quad L_{nacelle} = L_{eng} + 1.5D_{eng} = 16.4 \text{ ft} \quad (4.10)$$

In civil aircraft, nacelles are invariably externally pod-mounted, either slung under or mounted over the wing or attached to the fuselage. A standard engine installation for business jet is the aft-fuselage mount, usually with a T-tail. This eliminates the wing-interference effects of wing-mounted engines and allows a short landing gear. Larger aircraft have nacelle pods mounted under the wing, but low-wing small aircraft have fuselage-mounted nacelle pods because there is insufficient ground clearance.

Engines mounted at the rear of the fuselage structure avoid the ground clearance problem but introduces other difficulties: aircraft centre of gravity moves aft, leading to requirement of the wing to be moved back to balance the aircraft and consequently demands larger control surfaces, and also it increases the cabin noise at the rear of the aircraft (reason for which there are no seats in the rear part).

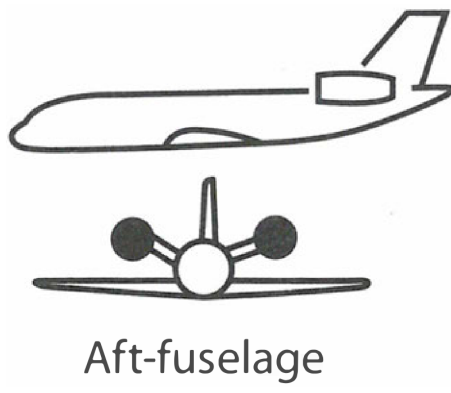


Figure 4.6: Chosen configuration for engine

4.6 Landing gear

The tricycle landing gear arrangement is commonly used, with two main wheels located behind the center of gravity (c.g.) and a front wheel positioned ahead of the c.g. This configuration ensures ground stability, allows landing at larger crab angles, improves forward visibility, and enables a flat cabin floor. As aircraft weight increases, multiple wheels are used to distribute the load, with twin nosewheels providing control in case of a flat tire. It is also desirable to have multiple main wheels for safety purposes. For aircraft weighing between 50,000 and 150,000 lb (22,680-68,040 kg), two wheels per strut are typical. The landing gear length must be set to prevent the tail from hitting the ground during landing. The angle between the main wheel position and the c.g. should be greater than the tipback angle or 15 degrees, whichever is larger, to prevent tipping back on the tail. A nosewheel carrying over 20% of the aircraft's weight indicates the main gear is too far aft, while less than 5%

weight on the nosewheel results in insufficient traction for steering. The optimal range for nosewheel weight is around 8-15% for different c.g. positions. A strut-travel angle of about 7 degrees is desired for smooth ride quality, allowing the tire to move upward and backward when encountering bumps.

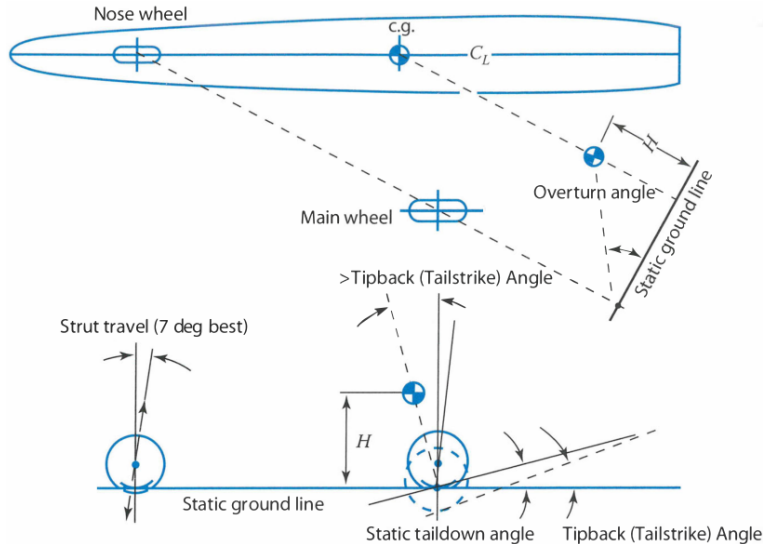


Figure 4.7: Tricycle landing-gear geometry

4.6.1 Main landing gear

For the main landing gear, consisting of two undercarriages, one for each half-wing, two wheels were provided on each side, for a total of 4. The weight acting on each wheel was calculated considering 90% of the MTOW, resulting in 23798 lb per wheel. The wheel dimensions in terms of diameter and width were calculated using the following statistical formulae:

$$D_{wh_{main}} = 1.63W_w^{0.315} = 39 \text{ inch} \quad w_{wh_{main}} = 0.1043W_w^{0.48} = 13 \text{ inch} \quad (4.11)$$

The results obtained, compared with the measurements of the reference aircraft, appear to be appropriate.

An important parameter for dimensioning the shock absorbers is the gear load factor, which is the average total load summed for all of the shock absorbers divided by the landing weight, and it is assumed to be constant during touchdown. The gear load factor determines how much load the gear passes to the airframe, which affects the airframe structural weight as well as crew and passenger comfort during the landing. Following Raymer's suggestion based on typical values for commercial aviation, N_{gear} was chosen equal to 2.7.

The efficiency of the shock absorber, assuming the use of an oleopneumatic type with metered orifice, was considered to be 0.75. The wheel efficiency, instead, is 0.47.

The vertical velocity (or "sink speed") at touchdown is established in various specifications for different types of aircraft. Most aircraft require 10 ft/s vertical velocity capability. This is

substantially above the 4-5 ft/s that most passengers would consider a "bad" landing. For tires it is assumed that the tire deflects only to its rolling radius, so the "stroke" (S_r) of a tire is equal to half the diameter minus the rolling radius, obtaining a value of 0.324 ft. Performing an energy balance between the kinetic energy developed at impact and the deformation work done by the shock absorber and the wheel tyre, the following equation is obtained:

$$\left(\frac{1}{2}\right) \left(\frac{W_{\text{landing}}}{g}\right) V_{\text{vertical}}^2 = (\eta LS)_{\text{shock,absorber}} + (\eta_T LS_T)_{\text{tire}}$$

from which it is possible to derive the shock absorber stroke of 0.648 ft.

By calculating the landing weight using weight fractions and MTOW and exploiting the gear load factor, it is possible to determine the average total load on the shock absorbers during deflection. This load (174650 lb), together with the internal pressure of the oleo (P), assumed to be a typical value of 259200 lb/ft², can be used to determine the internal and external diameters of the oleo.

$$D_{\text{int}} = \sqrt{2L_{\text{avg}}/(P\pi)} = 0.655 \text{ ft} \quad D_{\text{ext}} = 1.3D_{\text{int}} = 0.85 \text{ ft} \quad (4.12)$$

The remaining parameters to be determined are those required by the RDS software for the design of the landing gear and represented in the fig.4.8.

The length was set at 4 ft, in accordance with the dimension taken from the reference aircraft. Having defined a stroke ratio of 0.6 (typical value), the static deflection was calculated by multiplying the stroke of the shock absorber by the stroke ratio, resulting in a value of 0.389 ft. Finally, a typical value of 7 deg was chosen as the rake.

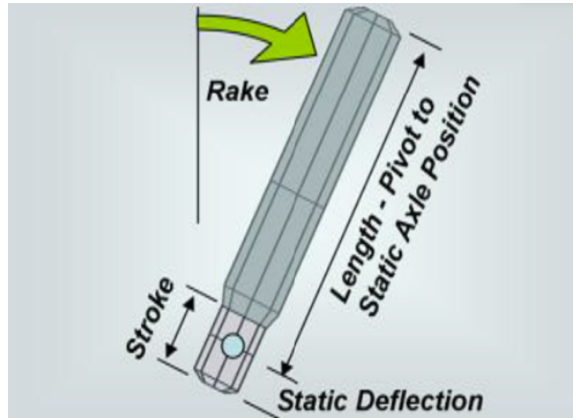


Figure 4.8: Main dimension parameters of the oleo strut shock absorber

4.6.2 Nose landing gear

For the nose landing gear, an entirely similar approach was followed, with a few differences: number of wheels equal to 2, 10% MTOW considered acting on the two wheels, different regression coefficients for calculating dimensions. The formulas used with the results obtained

are shown below.

$$W_w = 0.1W_0/N_{wh,nose} = 5288 \text{ lb} \quad D_{wh} = 24.3 \text{ inch} \quad w_{wh} = 6.39 \text{ inch} \quad (4.13)$$

$$D_{int} = 0.198 \text{ ft} \quad D_{ext} = 0.257 \text{ ft} \quad L_{nose} = 3 \text{ ft} \quad (4.14)$$

4.6.3 Landing gear drag

Once the undercarriage elements have been dimensioned, it is possible to estimate the value of C_{D0} relative to the landing gear extraction, to be considered in the take-off and landing phases for the performance calculation. To do this, it is possible to consider the ratio $(D/q)/A_f$, which is the ratio between drag and dynamic pressure divided by the frontal area of the different objects constituting the landing gear assembly. This value is called the miscellaneous parasite drag coefficient, and its values is 0.25 for both the wheels and the strut. Note that landing-gear drag is actually a function of lift. The more lift the aircraft wing is producing, the greater the velocity of the airflow over the top of the wing and, conversely, the lesser the airflow velocity underneath the wing where the gear is located. Hence, at higher lift coefficients the gear drag is reduced. This can be ignored for initial analysis.

In fact, it was sufficient to estimate the frontal areas of the various elements and multiply these values by the respective miscellaneous parasite drag coefficient. Results are shown below.

$$(D/q)_{main,wh} = 5.65 \text{ ft}^2 \quad (D/q)_{nose,wh} = 1.95 \text{ ft}^2$$

$$(D/q)_{main,st} = 2.78 \text{ ft}^2 \quad (D/q)_{nose,wh} = 0.625 \text{ ft}^2$$

D/q has units of square feet, and so is sometimes called the "drag area." D/q divided by the wing reference area yields the miscellaneous parasite drag coefficient. Then the sum of all D/q was multiplied by a surplus coefficient of 1.2 and divided by the wing area, yielding a final C_{D0} of 0.0109.

4.7 Design Layout

The results obtained in this section were used as data input for the realization of the preliminary sketch, using a specific software called RDSwin student (developed by Raymer). In following pages top, front, side and isometric views obtained by RDSwin design module are illustrated. A spreadsheet contains all dimensions for individual components, providing essential information on wetted area.

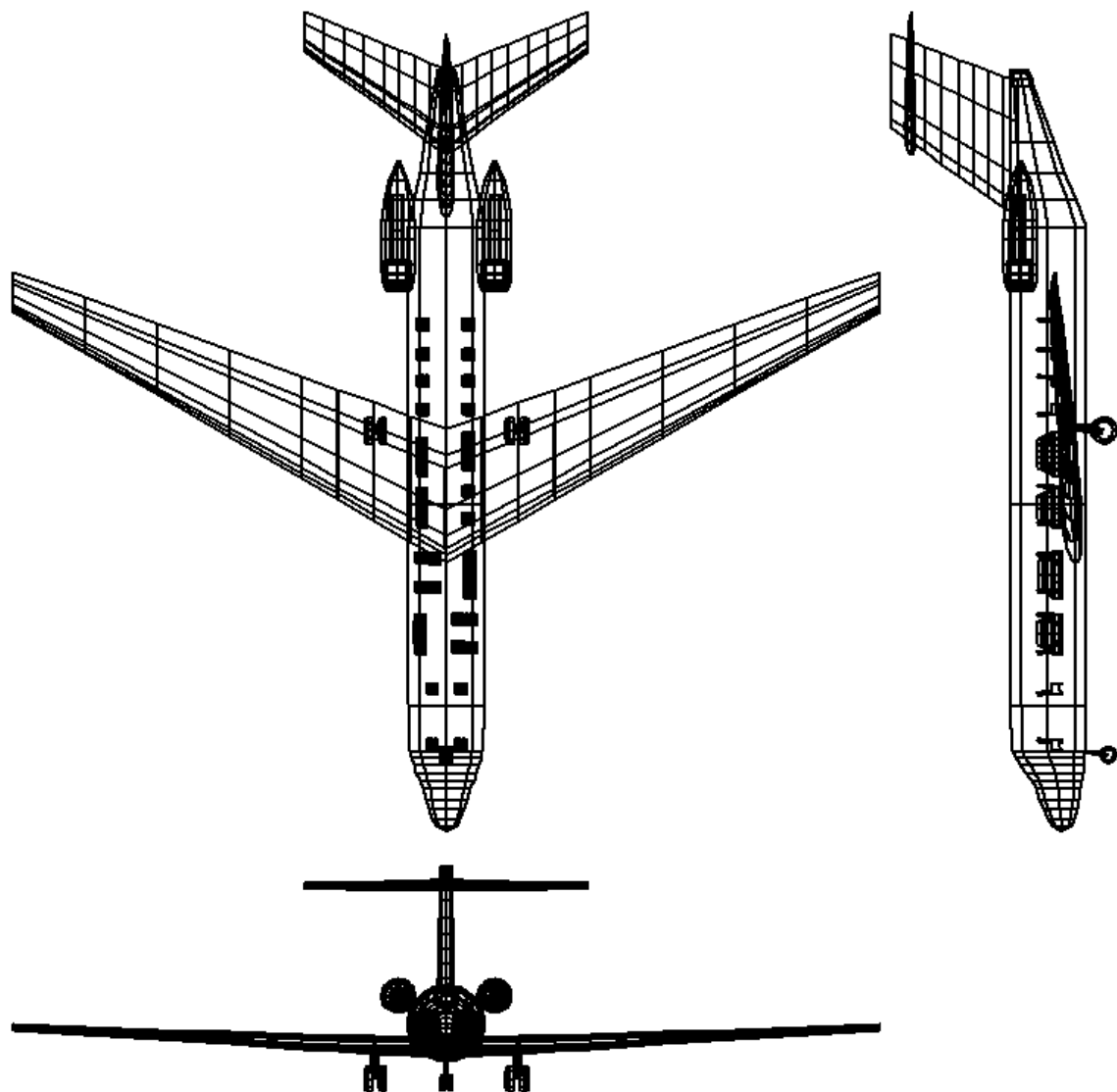


Figure 4.9: Orthographic view

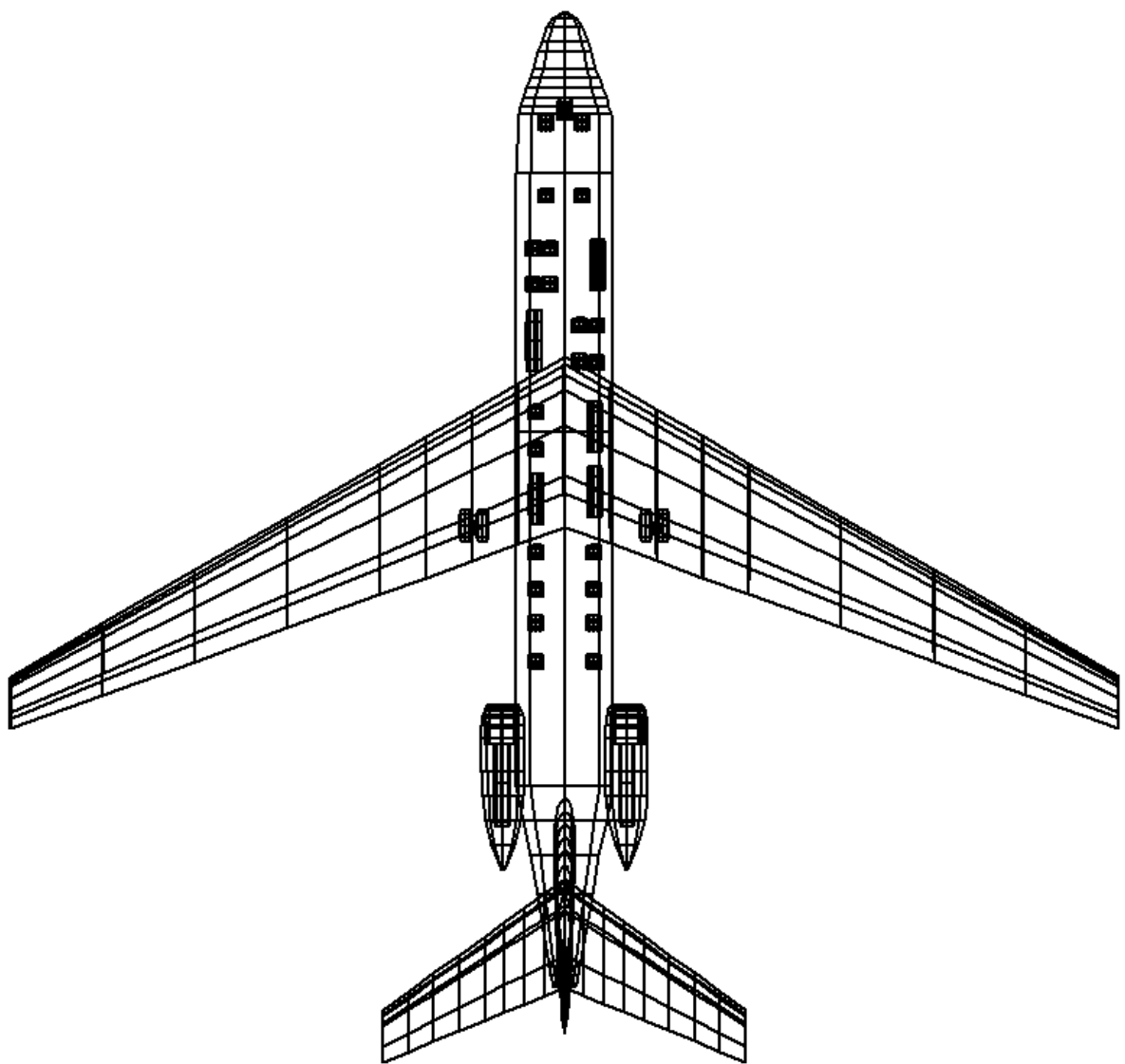


Figure 4.10: Top view

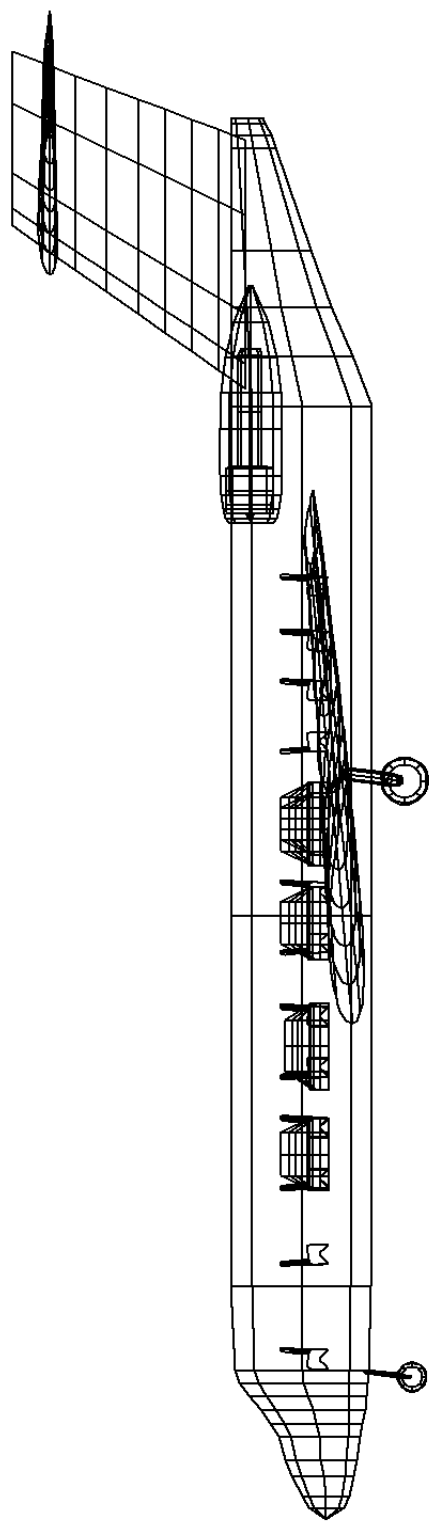


Figure 4.11: Side view

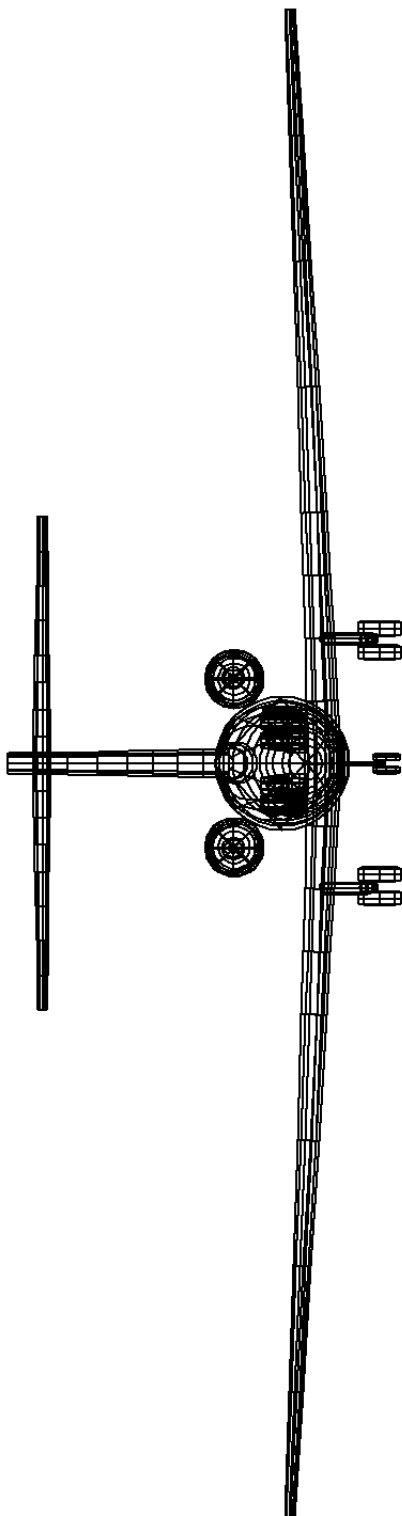


Figure 4.12: Front view

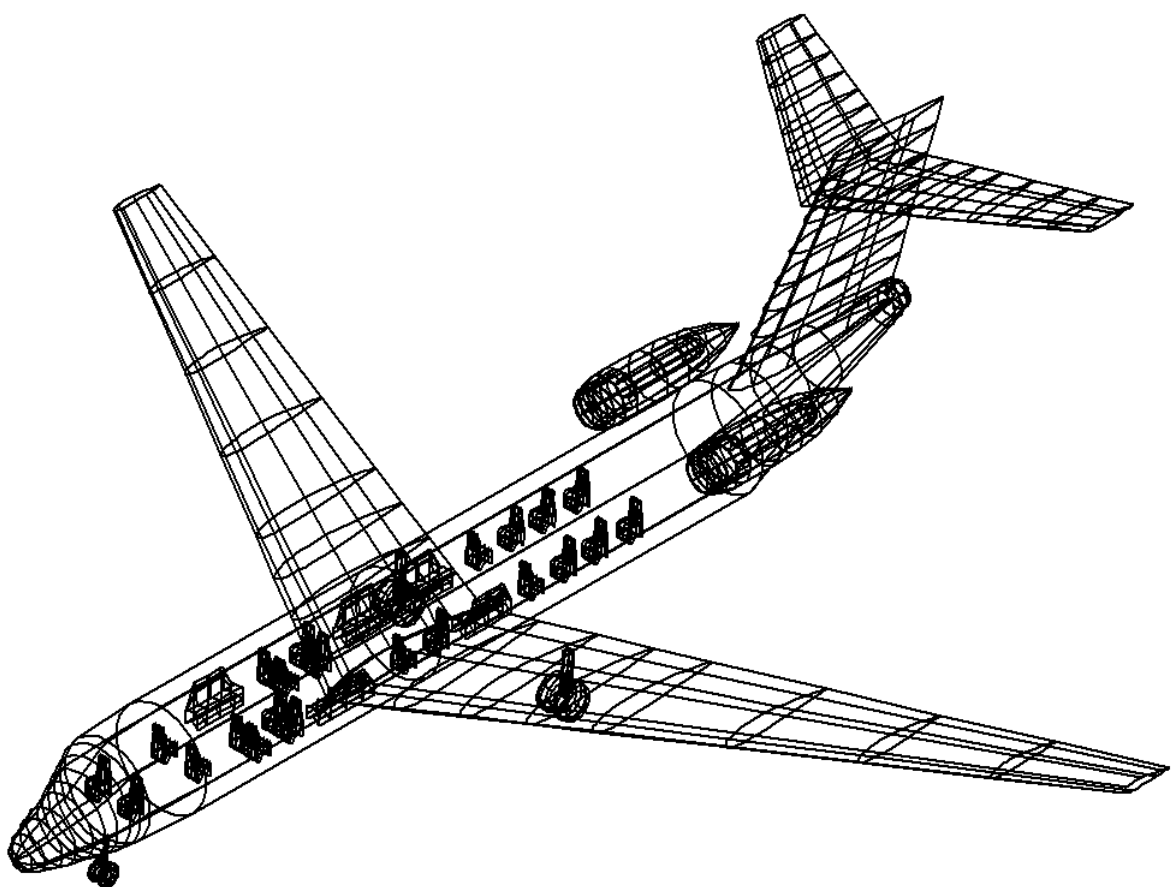


Figure 4.13: Isometric view

Chapter 5

Analysis

5.1 Aerodynamic analysis

Starting from the sketch geometry created, and from the data of the airfoils selected for the aerodynamic surfaces, an aerodynamic analysis can be conducted using the RDS software. The data obtained from this analysis will be useful for the subsequent performance check made in the last chapter, as they provide more precise information on terms that had hitherto only been derived on the basis of statistical or first-attempt estimates. An integrated tool allows

AERO DATA		WING		FUSELAGE		VERTICAL TAIL	
Max V or M#	516.37	# Components	1.	# Components	1.	# Components	1.
Max Altitude	46000.	Sref-wing	1214.4	Swet	2587.11	S-tail	235.8
% Laminar(all)	0.0	Sexp-wing	1218.43	length	96.9	Sexp-tail	236.65
k/10^5	2.08	A true	10.	diam-effctiv	9.6688	A true	1.1
%Leak&Protub	2.	A effective	10.	Q (interfer)	1.	A effective	1.1
Amax-aircraft	202.87	Lambda Ct/Cr	0.3	Upsweep deg	10.	Lambda Ct/Cr	0.7
length-eff	104.31	Sweep-LE	30.	Base Area	0.0	Sweep-LE	35.
Ewd	0.0	t/c average	0.14	Windshield Af	20.	t/c average	0.12
CL-cruise	0.6782	Delta Y	3.6	MiscD/q	0.0	Delta Y	3.
%WD Flatness	0.0	Q (interfer)	1.	Nose Length	0.0	Q (interfer)	1.
(n/a)	0.0	CL-design	0.5	X-front	0.0	(n/a)	0.0
MnvrFlapdClimax	0.0	CLmx-airfoil	1.5	(n/a)	0.0	(n/a)	0.0
set F*(Sexp/S)	0.95	% Laminar	80.	% Laminar	50.	% Laminar	80.
DragFudge(all)	0.0	DragFudge	1.	DragFudge	1.	DragFudge	1.
NACELLE		HORIZONTAL TAIL					
# Components	2.	# Components	1.				
Swet-nac	180.9	S-tail	287.24				
length	16.353	Sexp-tail	288.47				
diam-effctiv	4.2695	A true	4.5				
Q (interfer)	1.	A effective	4.5				
Upsweep deg	0.0	Lambda Ct/Cr	0.47				
Abase	3.	Sweep-LE	36.112				
(n/a)	0.0	t/c average	0.12				
MiscD/q	0.0	Delta Y	3.				
(n/a)	0.0	Q (interfer)	1.				
(n/a)	0.0	Dihedral	0.0				
(n/a)	0.0	(n/a)	0.0				
% Laminar	0.0	% Laminar	80.				
DragFudge	1.	DragFudge	1.				

Figure 5.1: Aerodynamics RDS data: Conventional airfoil method (FPS units)

the calculation of the total parasite drag coefficient for each step of 10000 ft altitude until the ceiling condition, including the effect of the Mach variation (from 0.2 to 1). The resulting

CHAPTER 5. ANALYSIS

text file is shown in figure 5.2 which has been cleaned from the original output to show the C_{D0} values corresponds respectively to the takeoff condition and at the two altitudes of 30000 ft and 4000 ft from which from the graph it is then possible to interpolate the exact value to the actual flight altitude which is equal to $C_{D0} = 0.0165$. The plot generated instead is shown in figure 5.3. The component buildup method estimates the subsonic parasite drag of each

PARASITE DRAG CALCULATION (results in drag counts - 10000xCdo)								
Reference Area = 1214.40 sq-ft								
Altitude =	0.	ft	Mach = 0.20	Velocity	132.3	kts	S-wet	Cdo
WING	1	17.124	8.055	1.318	1.000	1.000	2497.5	22.3
FUSELAGE	1	137.335	10.712	1.085	1.000	1.000	2587.1	67.1
Includes:		Upsweep= 29.5		Windshield= 11.5				
VERT TAIL	1	20.961	7.651	1.261	1.040	1.000	482.6	4.1
NACELLE	2	23.177	26.247	1.091	1.000	1.000	180.9	20.4
Includes:		Base= 11.5						
HORZ TAIL	1	11.811	8.920	1.261	1.040	1.000	588.3	5.8
			TOTAL PARASITE DRAG COEFFICIENT				Cdo	119.6
Altitude = 30000.	ft		Mach = 0.80	Velocity	471.5	kts	S-wet	Cdo
WING	1	27.584	6.869	1.412	1.000	1.000	2497.5	20.3
FUSELAGE	1	221.227	9.459	1.054	1.000	1.000	2587.1	63.5
Includes:		Upsweep= 29.5		Windshield= 11.5				
VERT TAIL	1	33.765	6.530	1.366	1.040	1.000	482.6	3.8
NACELLE	2	37.335	23.160	1.059	1.000	1.000	180.9	33.5
Includes:		Base= 25.5						
HORZ TAIL	1	19.026	7.564	1.351	1.040	1.000	588.3	5.3
			Drag rise or Wave Drag coeff				Cdw	36.2
			TOTAL PARASITE DRAG COEFFICIENT				Cdo	162.6
Altitude = 40000.	ft		Mach = 0.80	Velocity	458.9	kts	S-wet	Cdo
WING	1	18.496	7.621	1.412	1.000	1.000	2497.5	22.6
FUSELAGE	1	148.344	10.060	1.054	1.000	1.000	2587.1	64.9
Includes:		Upsweep= 29.5		Windshield= 11.5				
VERT TAIL	1	22.641	7.226	1.366	1.040	1.000	482.6	4.2
NACELLE	2	25.035	24.588	1.059	1.000	1.000	180.9	34.0
Includes:		Base= 25.5						
HORZ TAIL	1	12.758	8.432	1.351	1.040	1.000	588.3	5.9
			Drag rise or Wave Drag coeff				Cdw	36.2
			TOTAL PARASITE DRAG COEFFICIENT				Cdo	167.6

Figure 5.2: Some RDS C_{D0} aerodynamics results

component of the aircraft using a calculated flat-plate skin friction drag coefficient C_f and a component from factor FF that estimates the pressure drag due to viscous separation. Then the interference effects on the component drag are estimated as a factor Q . Miscellaneous drag $C_{D_{misc}}$ for flaps and base area are then estimated and added to the total, along with estimated contributions for leakages and protuberances $CD_{L\&P}$. So, the subsonic parasite drag buildup is calculated by equation 5.1.

$$C_{D0subsonic} = C_{D_{misc}} + C_{DL\&P} + \frac{\sum(C_{fc}FF_cQ_cS_{wetc})}{S_{ref}} \quad (5.1)$$

The flat plate skin friction coefficient depends upon the Reynolds number, Mach number and skin roughness. The most important factor affecting skin friction drag is the extent to which the aircraft has laminar flow over its surface. RDS allows each component to have a different estimate of the laminar flow percentage or allows a single percent estimate for the whole aircraft (input column Aero Data). By reference [1] we chose 50% for fuselage and 80%

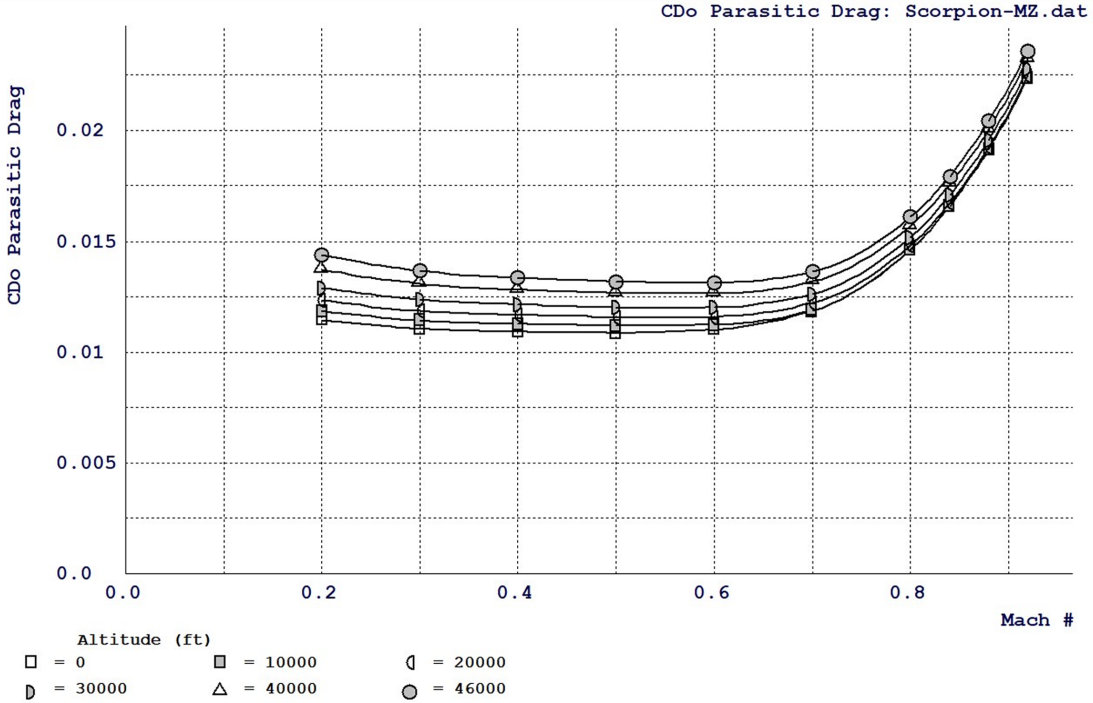


Figure 5.3: C_{D0} vs Mach number plot for different flight altitudes

for wing and tails. So, the flat plate skin friction coefficient for each components is calculated interpolating between turbulent and laminar values. For the laminar C_f depends on Reynolds number while the turbulent C_f depends on cut-off Reynolds number which accounts the effect of skin roughness k on the friction coefficient. Components form factor is calculated for each component relating to its geometrical dimensions. Parasite drag is increased due to the mutual interference between components. We considered this parameter negligible as we do not yet have adequate information at this stage of the project, so $Q = 1$. Most transport aircraft (as well as our) have a pronounced upsweep to the aft fuselage and this increase the drag beyond the value calculated by the fuselage form factor. RDS accounts this extra drag (D/q)_{upsweep} for the fuselage through the upsweep angle input and through the maximum cross sectional area of the fuselage taken from the sketch data.

Drag due to lift is calculated by the leading-edge suction method. It is a semi empirical method for estimation of K that allow for the variation of K with lift coefficient and Mach number. In 100% leading edge suction case the induced drag constant K: a 3-D wing is considered to have 100% leading edge suction when the Oswald efficiency factor exactly equals 1.0. In 0% leading edge suction case the induced drag constant K is calculated by equation 5.2.

$$K_{100\%} = \frac{1}{\pi AR} \quad K_{0\%} = \frac{1}{C_{L\alpha}} \quad (5.2)$$

The real percent of leading edge suction attained by the wing depends largely upon the leading edge radius, the sweep, the wing design lift coefficient and the actual lift coefficient. For any wing, the value of S is at a maximum when the wing is operating at the design lift coefficient.

For most wing, S equals approximately 0.9 when operating at the design lift coefficient. The input design lift coefficient ($C_{L_{design}}$) is used to select the leading edge suction schedule. Since an NACA 2414 airfoil is adopted, the design lift coefficient equals 0.5. So, the induced drag factor and the Oswald's efficiency are calculated by 5.3:

$$K = SK_{100\%} + (1 - S)K_{0\%} \quad e = \frac{1}{(\pi AR/C_{L\alpha})(1 - S) + S} \quad (5.3)$$

Subsonic $C_{L\alpha}$ is calculated with equation 5.4 and approximating the airfoil efficiency η was

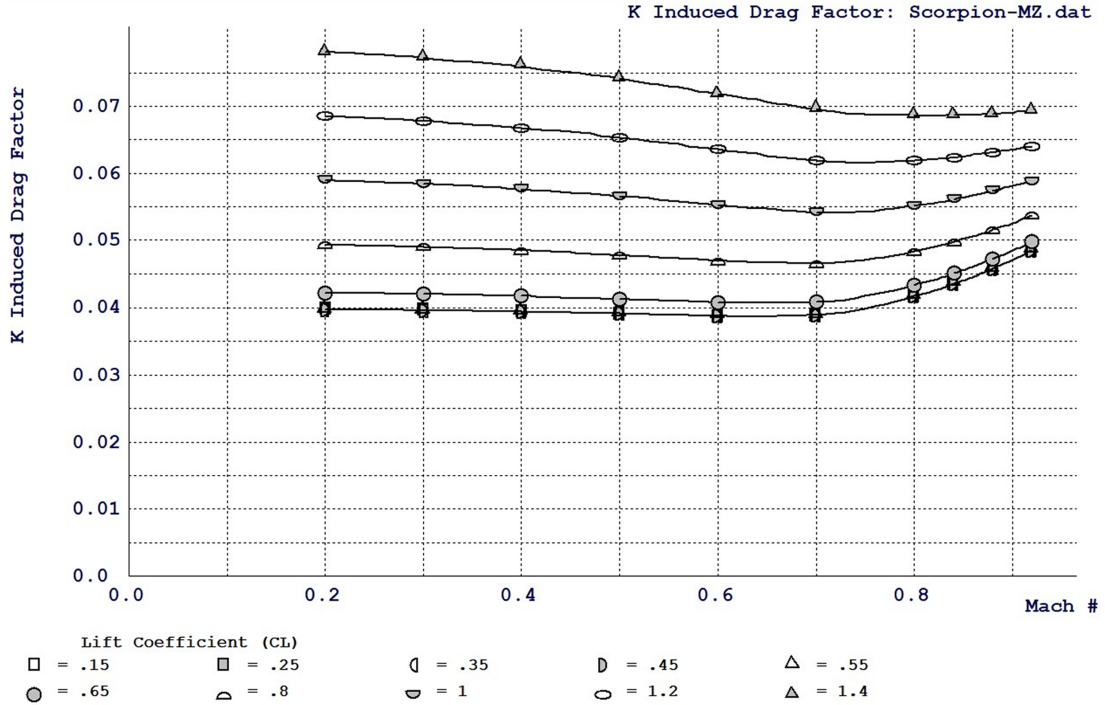


Figure 5.4: Induced Drag Factor (K) plot

set about 0.95. S_{ref} , $S_{exposed}$ and Λ_{max} values are taken from layout file. Furthermore, $\beta^2 = 1 - M^2$.

$$CL_\alpha = \frac{2\pi AR}{2 + \sqrt{4 + \frac{AR^2\beta^2}{\eta^2} \left(1 + \frac{\tan^2 \Lambda_{max}}{\beta^2}\right)}} \left(\frac{S_{exp}}{S_{ref}} \right) F \quad (5.4)$$

A key parameter in the analysis of wing lift curve slope as well as induced drag is the product $F(S_{exp}/S_{ref})$, which is the fuselage lift factor times the ratio of exposed to reference wing area. If this product is greater than one, it implies that the total lift of the actual wing plus the fuselage area covering the wing is greater than the lift of the trapezoidal wing itself. As a typical, conservative limit, 0.95 is suggested to use.

Maneuver flap ΔCl_{max} is added to Cl_{max} for LE suction K calculation, where the airfoil maximum lift coefficient Cl_{max} for a NACA 2414 is 1.5. We considered clean configuration only, so we left zero maneuver flaps contribution. The contribution made by the flaps will be evaluated later in the performance phase.

For illustrative purposes only, it can be said that in transonic flight, the shock formation interferes with leading edge suction. This increases the K value. When the leading edge becomes supersonic, the suction goes to zero so the K value equals the $K_{0\%}$ value. Some of the most significant plots generated with the software will be shown below.

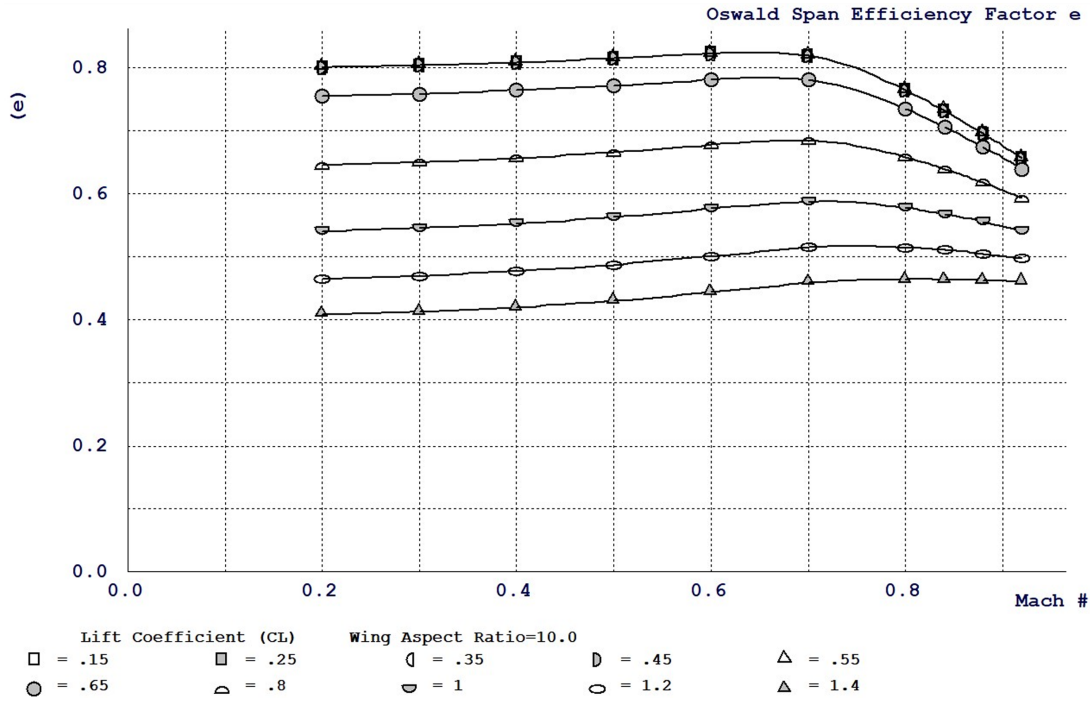


Figure 5.5: Oswald's efficiency plot

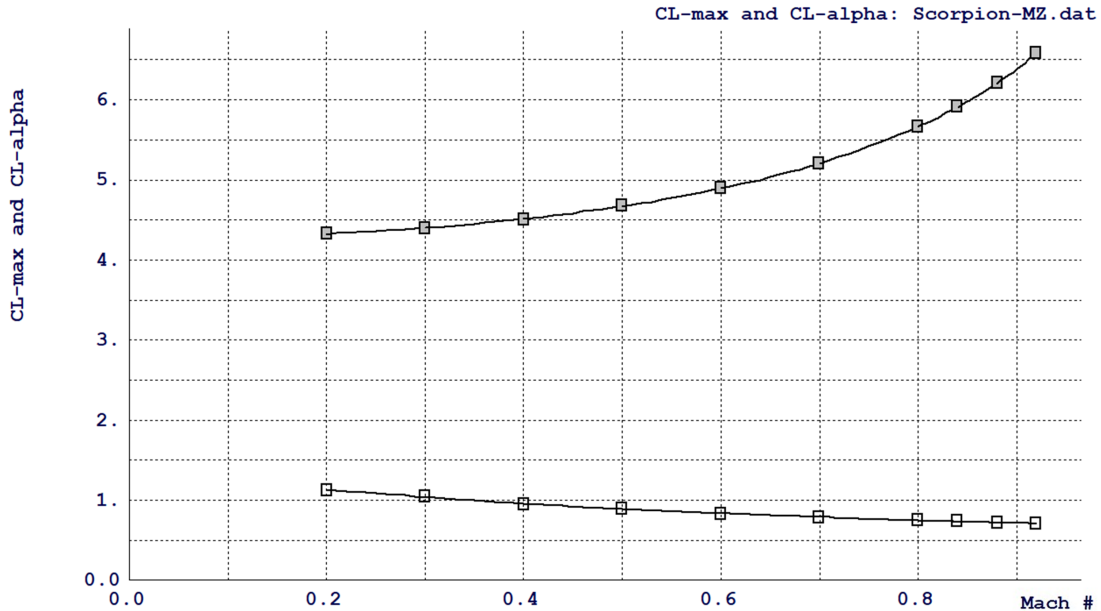


Figure 5.6: Lift curve slope and $C_{L_{max}}$ vs Mach Number

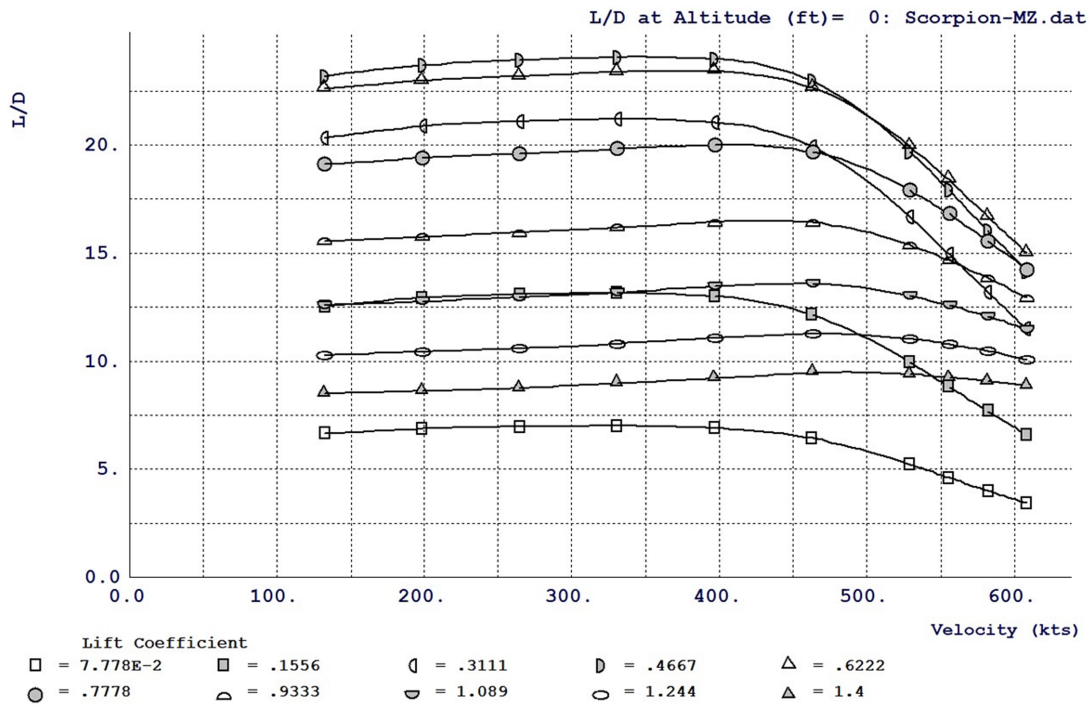


Figure 5.7: Lift-to-drag at sea level

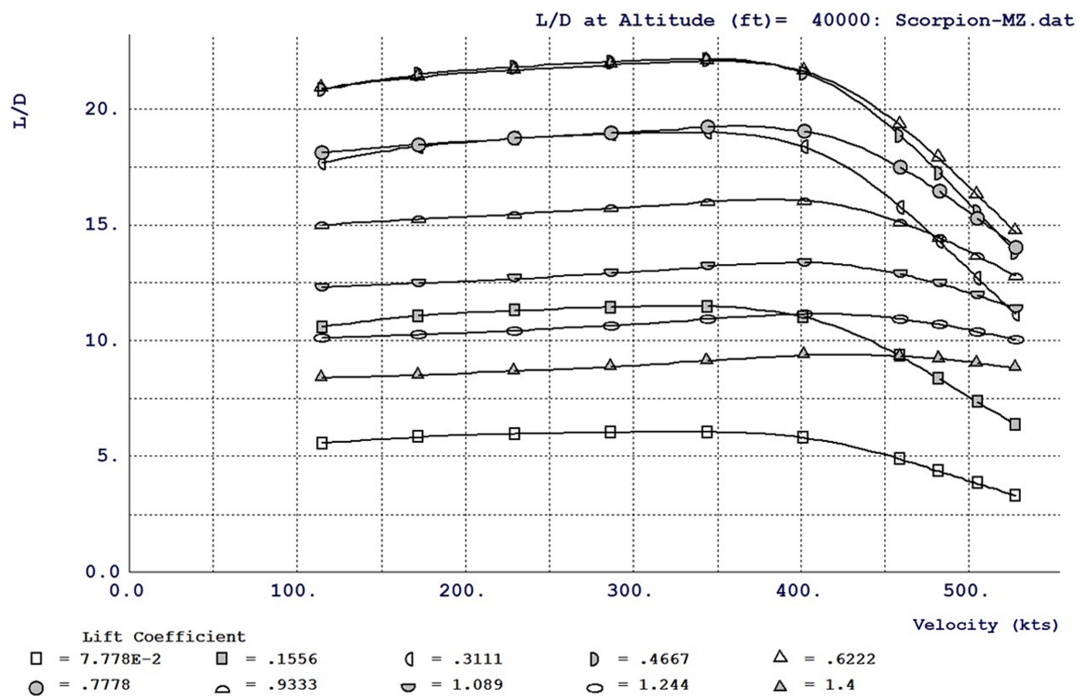


Figure 5.8: Lift-to-drag at 40000 ft

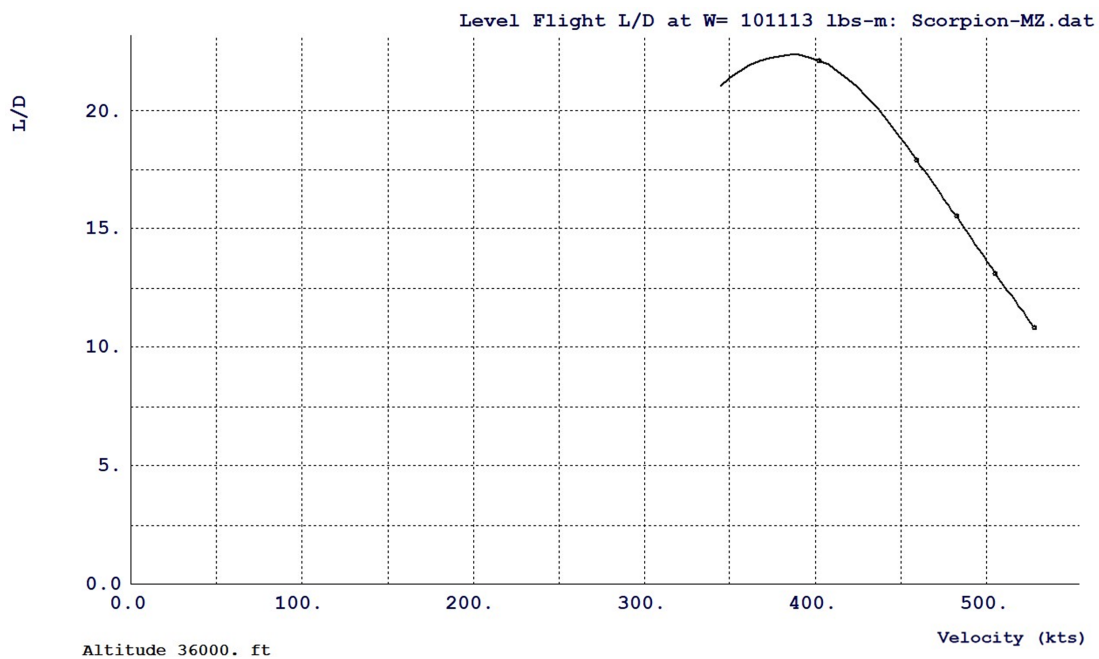


Figure 5.9: Lift-to-drag in level flight (36000 ft) at initial cruise condition

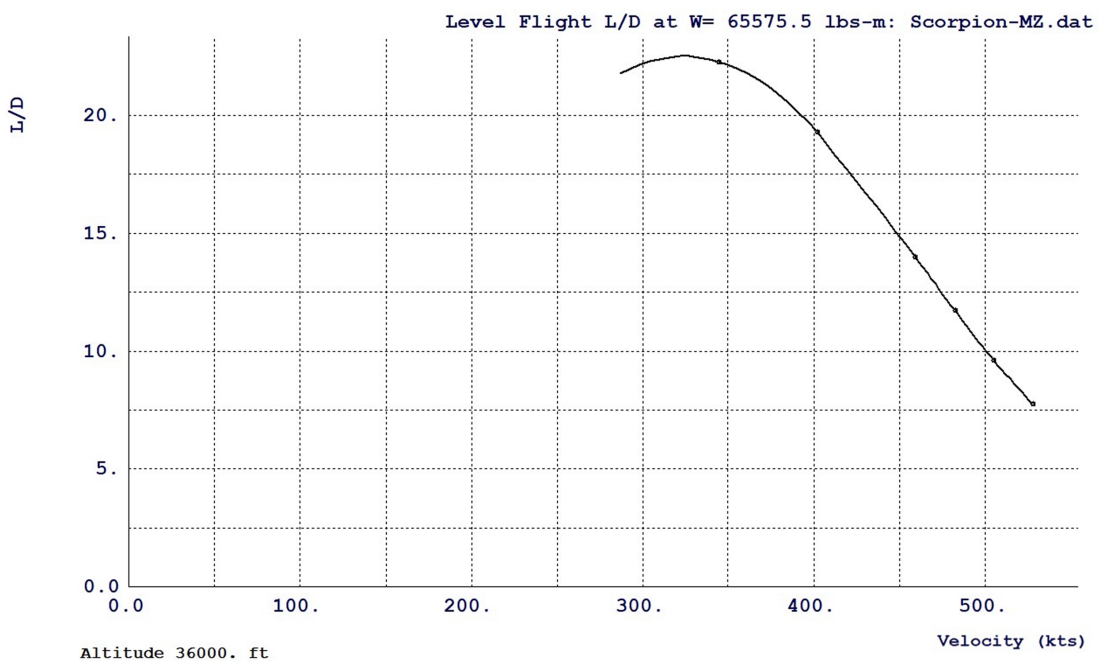


Figure 5.10: Lift-to-drag in level flight (36000 ft) at final cruise condition

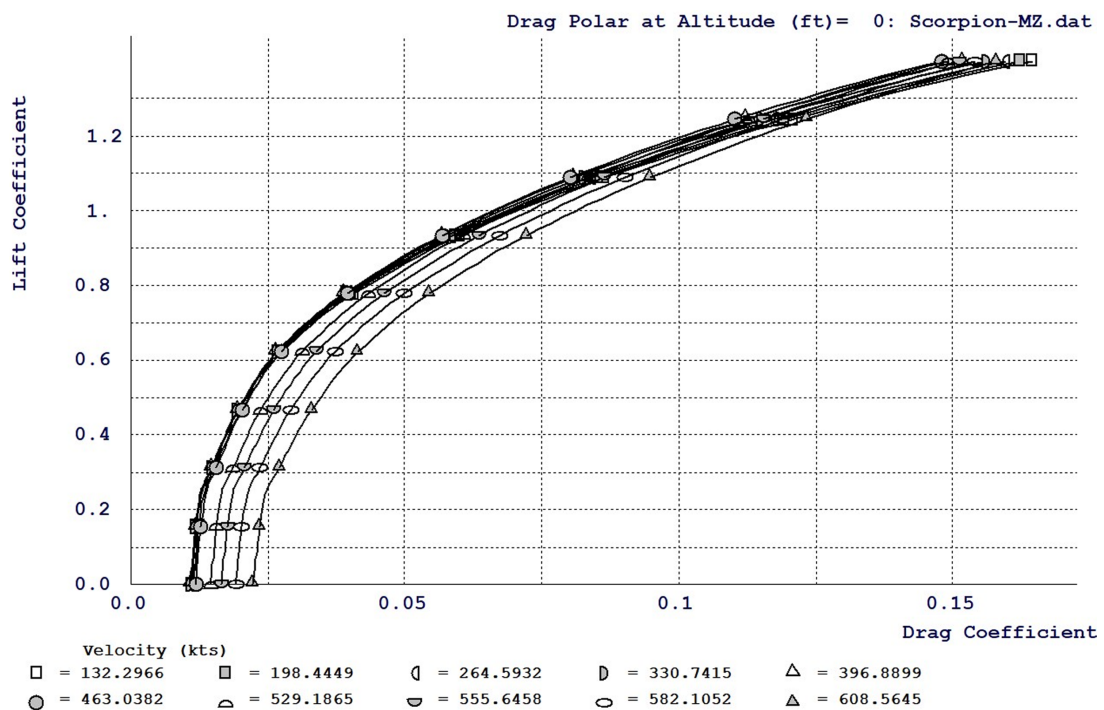


Figure 5.11: Drag polar at sea level

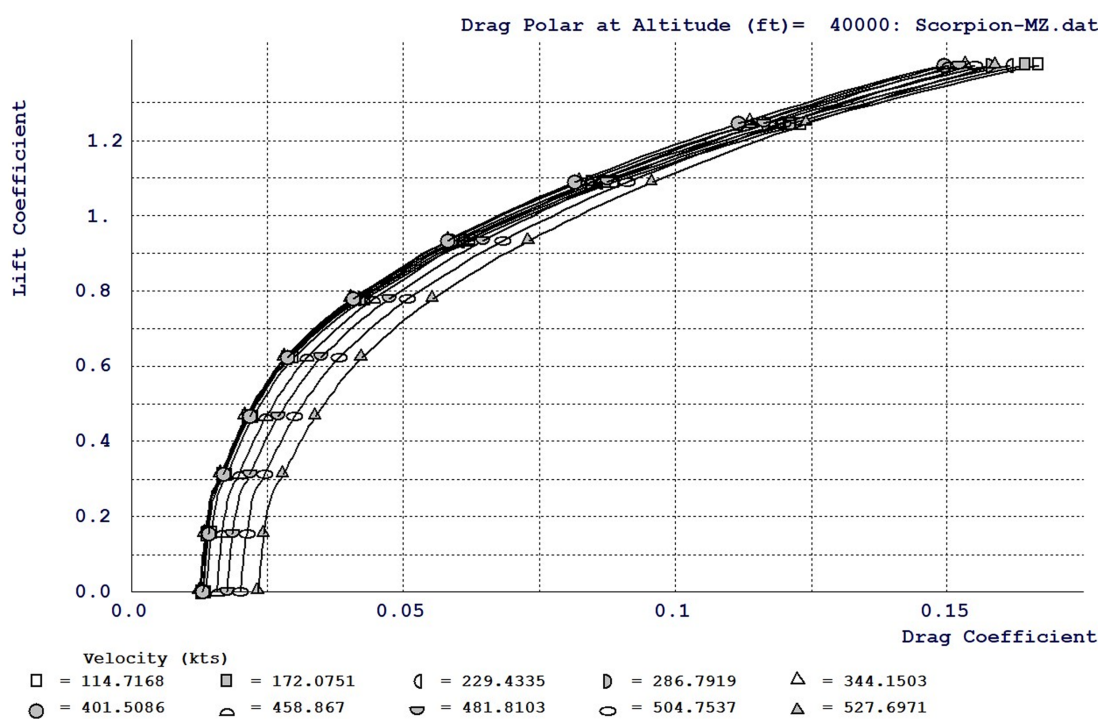


Figure 5.12: Drag polar at 40000 ft

5.2 Cost analysis

Cost estimation for new aircraft is primarily based on statistical analysis of past aircraft costs. However, comparing the costs of prior aircraft and predicting meaningful costs for future aircraft is challenging. One issue is deciding which type of currency to use for cost comparisons. Then-year dollars represent actual expenditures over time, while constant-year dollars adjust for inflation. Constant-year dollars are preferred for establishing cost baselines, but Congress budgets in then-year dollars. The quantity and production rates of aircraft also impact costs, as more production leads to learning curve benefits and lower costs. Additionally, different cost groupings are often used without proper identification, making comparisons between flyaway costs and program or life-cycle costs meaningless. Figure 5.13 shows the elements that make up aircraft life-cycle cost (LCC). RDT&E (research, development, test, and evaluation)

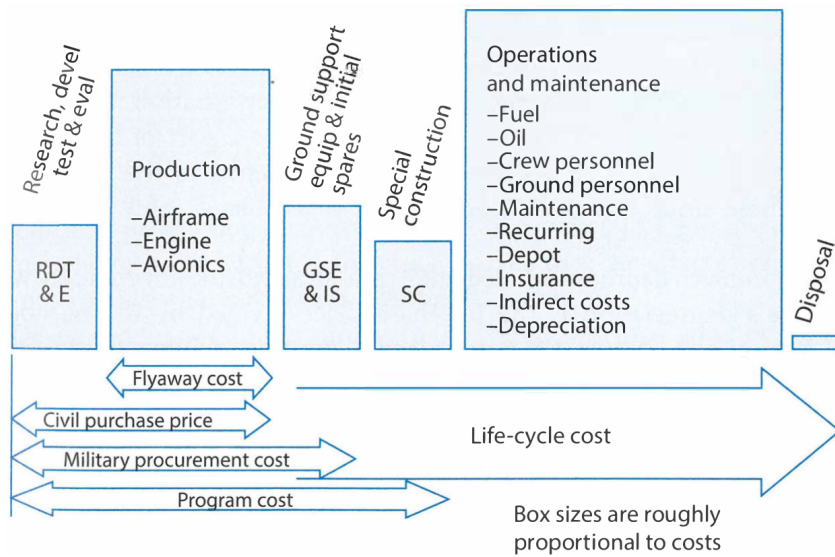


Figure 5.13: Element of life-cycle cost

encompasses the costs associated with technology research, design engineering, prototyping, testing, and evaluations for operational suitability. It includes certification costs.

The aircraft "flyaway" or production cost includes labor, materials, airframe, engines, avionics, and production tooling. Production costs are recurring and decrease per aircraft due to the learning-curve effect. Production costs make up about less than half of the life-cycle cost for commercial aircraft.

Operations and maintenance (O&M) costs cover fuel, oil, aircrew, maintenance, and indirect expenses, including insurance for civil aircraft. Depreciation, based on the purchase price and spread over several years, is considered an operating cost for commercial aircraft. The total life-cycle cost also takes into account the disposal of the aircraft, with civil aircraft often having a resale value representing a negative disposal cost.

During conceptual design, cost estimation relies on statistical methods known as "cost-estimating relationships" (CERs). These relationships are developed by analyzing cost data from multiple airplanes and correlating them with design parameters such as empty weight

and production quantity. CERs are often used to estimate labor hours rather than actual costs to account for labor rates and macroeconomic factors. Developing CERs involves obtaining a significant amount of normalized cost data and making adjustments to account for differences between design assumptions and existing aircraft. Cost analysts may use "fudge factors" to fine-tune the results obtained from the equations. CERs are developed by aircraft companies and customer organizations for evaluating proposed aircraft. The RAND Corporation has developed a widely used set of cost-estimating relationships (CERs) called DAPCA IV (Development and Procurement Costs of Aircraft) for conceptual aircraft design. DAPCA estimates the hours and costs associated with research, development, test, and evaluation (RDT&E) and production. It considers various cost elements and factors, such as engineering, tooling, manufacturing, quality control, development support, flight test, and manufacturing materials. Engineering hours encompass design, analysis, configuration control, and system engineering, primarily during RDT&E but with some effort in production. The equation for estimating engineering effort takes into account the production quantity. Tooling hours include preparation for production, such as tool design, fabrication, programming, and test apparatus development. Manufacturing labor covers the direct labor involved in aircraft fabrication, including subassembly, final assembly, routing, and purchased part installation. Quality control is estimated separately and involves inspection throughout the manufacturing process. The hours estimated by DAPCA are based upon the design and fabrication of an aluminum aircraft. For aircraft that are largely fabricated from other materials, the hours must be adjusted to account for the more difficult design and fabrication with a fudge factor. Predicted aircraft costs will be multiplied by an "investment cost factor" to determine the purchase price to the customer. The investment cost factor includes the cost of money and the contractor profit; it is considered highly proprietary by a company.

The RDT&E phase includes development support and flight-test costs. Development support costs include manufacturing support for RDT&E, such as mockup fabrication and structural test articles. Flight-test costs encompass planning, instrumentation, flight operations, data reduction, and engineering and manufacturing support. Manufacturing materials include the raw materials, purchased hardware, and equipment used in aircraft construction, except for engines and avionics. DAPCA assumes that the engine cost is known.

For RDT&E cost estimation, the first necessary step is to set a set of parameters needed to exploit the proposed statistical equations. These parameters are summarized in the table 5.1.

Parameter	Symbol	Value	Description
Production aircraft	Q	200	A production volume of 200 aircraft was assumed
Flight test aircrafts	FTA	3	Sacrificial aircraft for flight tests
Investment factor	IF	1.1	To evaluate the purchase price to the customer
Fudge factor	FF	1.4	Taking into account the presence of elements made of steel, titanium, carbon fiber and other composite materials

Table 5.1: First parameters chosen for cost estimation

Applying the equations of the DAPCA model, the following results were obtained for engineering, tooling, manufacturing and quality control hours. The effect of the learning curve, related to the number of aircraft produced, is contained within the statistic formulae. At this

Parameter	Symbol	Value (kh)	Evaluation
Engineering hours	H_{eng}	23487	$4.86(W_e^{0.777})(V_{max}^{0.894})(Q^{0.163})IF \cdot FF$
Tooling hours	H_{tool}	14274	$5.99(W_e^{0.777})(V_{max}^{0.696})(Q^{0.263})IF \cdot FF$
Manufacturing hours	H_{man}	55436	$7.37(W_e^{0.82})(V_{max}^{0.484})(Q^{0.641})IF \cdot FF$
Quality control hours	H_{qual}	11354	$0.133H_{man}IF \cdot FF$
Total hours	H_{tot}	104552	$H_{eng} + H_{tool} + H_{man} + H_{qual}$

Table 5.2: Total hours of work

point, the hourly cost for engineering, tooling, quality control and maintenance operations must be defined. They were estimated on the basis of the wrap rate values provided by Raymer, valid for 1986. However, several economic factors must be considered in order to define valid costs today. For this reason, it was decided to take the values provided by Raymer as the basic pay of the workers, multiplying them by a wrap rate factor of 1.8, in order to obtain a more reasonable estimate for the current year, without digressing too far into purely financial talk. The corresponding costs are obtained by multiplying the hours obtained by the hourly

Parameter	Symbol	Value (\$)
Engineering	R_{eng}	106
Tooling	R_{tool}	108
Quality control	R_{qual}	99
Manufacturing	R_{man}	90

Table 5.3: Wrap rates

costs, yielding the results in 5.4. The costs for development support, flight test, manufacturing

Parameter	Symbol	Value (k\$)
Engineering cost	C_{eng}	2489655
Tooling cost	C_{tool}	1541641
Quality control cost	C_{qual}	1124090
Manufacturing cost	C_{man}	4989258

Table 5.4: Labour costs

material and engine production were also calculated using the DAPCA formulae as in 5.5. DAPCA does not estimate avionics costs. They must be estimated from data on similar aircraft or from vendors' quotations. Avionics costs depends upon sophistication and can be approximated as \$4000-\$8000 per pound in 2012 dollars, as suggested by Raymer. Considering that the upper bound of the cost per pound refers to the sophisticated avionics of a military fighter, a value of \$4500/pound has been set for a business jet. The weight of the avionics was obtained using a statistical formula that considers a fraction of the empty weight. The final

Parameter	Symbol	Value (k\$)	Evaluation
Devel. support cost	C_{dev}	151717	$45.42(W_e^{0.63})(V_{max}^{1.3})$
Flight test cost	C_{ft}	28047	$1243.03(W_e^{0.325})(V_{max}^{0.822})FTA^{1.21}$
MFG materials cost	C_{mfgm}	882872	$11(W_e^{0.921})(V_{max}^{0.621})(Q^{0.799})$
Engine prod. cost	C_{engine}	447350	$1548(0.043T_{req}/2 + 243.25M_{max} + 388)Q$

Table 5.5: Other costs

result, which is valid for a single aircraft, needs to be multiplied by the number of aircraft built. It was not possible to include the influence of the learning curve as this is considered within the design hours, which in the case of avionics is not provided.

$$W_{avionics} = 0.04W_e = 2286 \text{ lb} \quad C_{avionics} = 4500W_{avionics} = 10290 \text{ k\$/plane} \quad (5.5)$$

DAPCA does not include an allowance for the cost of interiors for passenger aircraft, such as seats, luggage bins, closets, lavatories, insulation, ceilings, floors, walls, and similar items. For a business jet, which is supposed to have a high-end interior in terms of luxury and comfort, a cost of \$6000 per passenger was assumed, considering that Raymer suggests a cost of \$3500 per passenger for a jet transport.

$$C_{interior} = 6000 \cdot N_{pax} = 108 \text{ k\$/plane} \quad (5.6)$$

The total cost of the aircraft is determined using the 5.7.

$$\begin{aligned} C_{aircraft} = & (H_{eng}R_{eng} + H_{tool}R_{tool} + H_{man}R_{man} + H_{qual}R_{qual} + C_{dev} \\ & + C_{ft} + C_{mfgm} + C_{engine}N_{eng} + C_{avionics} + C_{interior})/Q = 70905376\$ \end{aligned} \quad (5.7)$$

This cost has to be multiplied by the investment factor in order to obtain the sales price.

$$\text{AIRCRAFT PRICE} = C_{aircraft} \cdot \text{IF} = 77995914\$ \quad (5.8)$$

Considering the sale price of the reference aircraft, around \$70 million, it was found that the ScorpionMZ is priced around \$8 million higher. The estimate made, however, is supposed to be conservative in relation to the status of the project, which is still at the conceptual stage. Furthermore, for avionics and interiors, no regression formulae were used based on collected data, but rather a reasoning based on price/lb or price/passenger. In fact, by lowering the price of these two subsystems, global price would meet the cost of the G650ER. In any case, the DAPCA model provided a number that is in the same order of magnitude as the price of the reference aircraft.

5.2.1 Airline economic analysis and life cycle cost

O&M (Operations and Maintenance Costs) costs are determined from assumptions as to how the aircraft will be operated. The main O&M costs are fuel, crew salaries, and maintenance. The actual missions will rarely resemble the design mission. To estimate yearly fuel usage, a typical mission profile is selected, and the total duration and fuel burned are used to determine the average fuel burned per hour. This is multiplied by the average yearly flight hours per aircraft, which must be assumed based upon typical data for that class of aircraft. For business jets, Raymer suggests a range of 500-2000 hours/year/aircraft.

In order to get a complete picture of airline economics, we wanted to deal with it through a parametric approach. Therefore, several typical situations were evaluated, depending on the average annual flight hours, the typical range and above all by considering the individual cost of tickets as a variable, so that the resulting break-even (following the approach of a typical airline) is no longer a single value but will be a function of several variables. Furthermore, since business jets often do not follow the typical revenue policy of civil airlines, a revenue policy was also considered based on rental as a function of both the operating cycles conducted and the typical range.

An operating life of 20 years was considered for all analyses. Furthermore, the total amount of fuel burned per year of operation is multiplied by the fuel price, which was set to 0.32 \$/lb. Oil costs can be ignored.

The cost of a civil-aircraft crew (including flight and cabin crew) can be statistically estimated based upon the yearly "block hours." Block hours measure the total time the aircraft is in use, from when the "blocks" are removed from the wheels at the departure airport to when they are placed on the wheels at the destination. For a long-range aircraft, the block hours equal approximately the flight hours. Crew cost per block hour were estimated using the following approach. Raymer provides equations that are valid for a crew of 2 or 3 people in 5.9. V_{cr} is the cruise velocity in kt and W_0 is the takeoff gross weight in lb. The coefficients A, b take into account the dollar currency as of 2012.

$$n - \text{people crew cost} = A \left(V_{cr} \frac{W_0}{10^5} \right)^{0.3} + b \quad (5.9)$$

Since the ScorpionMZ crew comprises 4 persons, assuming a linear growth of these coefficients

Crew members	A	b
2	70.4	168.8
3	94.5	237.2

as a function of the number of persons, the following results were obtained. Obviously, the

Crew members	A	b
4	118.6	305.6

total annual crew cost comes from the product between crew cost block hours and typical flight hours considered. The cost of aircraft maintenance can be categorized into unscheduled maintenance and scheduled maintenance. Unscheduled maintenance costs depend on the frequency of breakdowns and the average cost of repairs. Scheduled maintenance is based on the number of items requiring regular maintenance and the associated frequency and cost. Maintenance activities are typically scheduled based on accumulated flight hours or flight cycles for commercial aircraft. The measure of maintenance efficiency is maintenance man-hours per flight hour (MMH/FH), with values ranging from 3 to 6 for business jets. Reducing MMH/FH is a design objective. The weight of the aircraft affects MMH/FH due to parts count and complexity, while aircraft utilization impacts the frequency of scheduled maintenance. Maintenance man-hours per year can be estimated from MMH/FH and flight hours per year, and labor costs are determined using labor wrap-rates from airline sources or approximated using manufacturing wrap-rates. For civil aircraft the following equations for materials cost per flight hour and per cycle can be used. The number of cycles per year is estimated by determining the total yearly block time divided by the block time per flight. The total materials cost is the cost per flight hour times the flight hours per year, plus the cost per cycle times the cycles per year.

$$MH/FH = 6 \quad MMH = (MMH/FH)FH_{avg}$$

$$C_{mat, FH} = 3.3 \left(\frac{C_{aircraft} - N_{eng}C_{engine}/Q}{10^6} \right) + 7.04 + 58 \left(\frac{C_{engine}}{Q \cdot 10^6} \right) - 13)N_{eng}FH_{avg} \quad (5.10)$$

$$\text{cycle} = FH_{avg}/hr_{flt_{typical}}$$

$$C_{mat,cycle} = (4((C_{aircraft} - N_{eng}C_{eng}/Q)/10^6) + 4.6 + (7.5(C_{eng}/Q/10^6) - 2.8)N_{eng}) \cdot \text{cycle} \quad (5.11)$$

$$C_{material} = C_{mat,cycle} + C_{mat, FH}$$

Insurance costs for commercial aircraft add approximately 1-3% to the cost of operations which are calculated as:

$$C_{operational} = 1.01(C_{material} + C_{labor,main.} + C_{crew} + C_{fuel})$$

The cost-effectiveness of an airliner is determined by its ability to generate revenue exceeding operating costs. Operating costs are divided into direct operating costs (DOC) and indirect operating costs (IOC). DOC costs include fuel, crew, maintenance, depreciation, insurance, and landing fees. Landing fees are often proportional to the aircraft's weight and can be a significant expense. Carbon taxes may also be imposed on airlines. DOC costs are measured as "cost per seat-mile" and used for comparing aircraft. IOC costs include depreciation of ground facilities, sales and customer service expenses, and administrative and overhead costs. Estimating IOC costs is challenging as they depend on the airline's operational choices. IOC costs are not easily statistically analyzed and have little dependence on aircraft design. They typically range from one-third to equal DOC costs, but the variation is significant. Reliable

IOC cost data is best obtained directly from airlines for economic analysis.

$$\begin{aligned} \text{DOC} &= C_{\text{operational}} & \text{DOC}_{\text{FH}} &= \text{DOC}/FH_{\text{avg}} \\ \text{IOC} &= \text{DOC} \cdot (2/3) & C_{\text{op,tot}} &= \text{DOC} + \text{IOC} & \text{LCC} &= C_{\text{aircraft}} + C_{\text{op,tot}} \cdot Y_{\text{life}} \end{aligned} \quad (5.12)$$

Airline revenue primarily comes from ticket sales, which are proportional to trip distance. Ticket prices are higher per mile for shorter distances and are usually sold in different classes, except for business jets that typically have a single premium class. Revenue estimation involves determining the average fare paid and the load factor, which measures the aircraft's occupancy. The load factor for break-even is calculated by dividing the cost per seat-mile by the average fare per seat-mile. Operating-cost break-even analysis considers direct operating costs (DOC) per seat-mile, while total-cost break-even analysis includes indirect operating costs (IOC) per seat-mile.

For each typical range considered and for each number of annual hours, the analyses performed are of two types:

- a first strategy is to find the breakeven curve that allows us to correlate the load factor with the ticket price; additionally, a lower price limit was considered below which a loss is incurred; this strategy assumes that the aircraft is operated as a civilian airliner, in which a factor such as load factor conditions the ticket price;
- the second strategy, on the other hand, follows the rental approach, which means that the price imposed by the owning company is not conditioned by the number of occupants; this scenario, which is quite common for business jets, correlates the minimum rental price with the number of cycles for every fixed typical range considering always 1500 FHPY. In Fig. 5.15, where the graphical results of the analysis are shown, some considerations need to be made regarding the graphs of the minimum rental price. The linear trend obtained is related to having defined indirect costs as a fraction of direct costs. The total operating costs, that is, the sum of direct and indirect costs, and thus the minimum rental cost, therefore, will simply grow proportionally with the number of cycles. Actually, indirect costs would deserve an appropriate discussion in order to derive an expression that can describe them appropriately.

The analysis results are shown below.

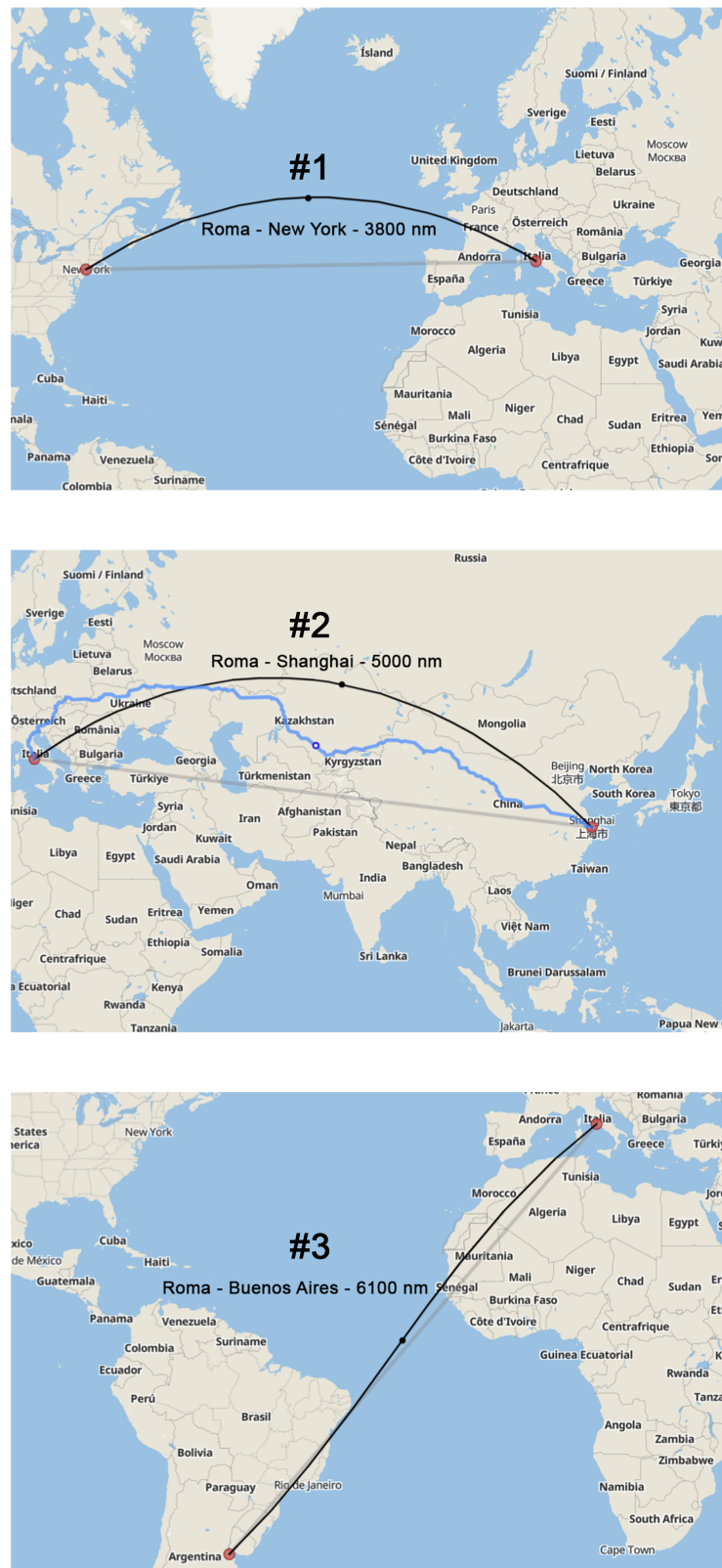


Figure 5.14: Typical mission considered

Parameter	Symbol	Value
Average flight hours	FHPY	1500
Typical flight range	$R_{typical}$	3800 nmi
Opeational life	$Y_{operational}$	20 years
Fuel cost (per year)	C_{fuel}	1684559 \$
Crew cost (per year)	C_{crew}	1596090 \$
Maint. labor cost	$C_{labor_{main.}}$	810000 \$
Insurance cost (per year)	C_{ins}	48805 \$
Total DOC (per year)	DOC	4880517 \$
Total IOC (per year)	IOC	3253678 \$
Total op. cost (per year)	$C_{operating}$	8134195 \$
Total life cycle cost	LCC	240679804 \$

Table 5.6: Typical mission #1 cost results

Parameter	Symbol	Value
Average flight hours	FHPY	1500
Typical flight range	$R_{typical}$	5000 nmi
Opeational life	$Y_{operational}$	20 years
Fuel cost (per year)	C_{fuel}	1558144 \$
Crew cost (per year)	C_{crew}	1596090 \$
Maint. labor cost	$C_{labor_{main.}}$	810000 \$
Insurance cost (per year)	C_{ins}	47406 \$
Total DOC (per year)	DOC	4740619 \$
Total IOC (per year)	IOC	3160413 \$
Total op. cost (per year)	$C_{operating}$	7901032 \$
Total life cycle cost	LCC	236016545 \$

Table 5.7: Typical mission #2 cost results

Parameter	Symbol	Value
Average flight hours	FHPY	1500
Typical flight range	$R_{typical}$	6100 nmi
Opeational life	$Y_{operational}$	20 years
Fuel cost (per year)	C_{fuel}	1470082 \$
Crew cost (per year)	C_{crew}	1596090 \$
Maint. labor cost	$C_{labor_{main.}}$	810000 \$
Insurance cost (per year)	C_{ins}	46446 \$
Total DOC (per year)	DOC	4644595 \$
Total IOC (per year)	IOC	3096397 \$
Total op. cost (per year)	$C_{operating}$	7740992 \$
Total life cycle cost	LCC	232815753 \$

Table 5.8: Typical mission #3 cost results

CHAPTER 5. ANALYSIS

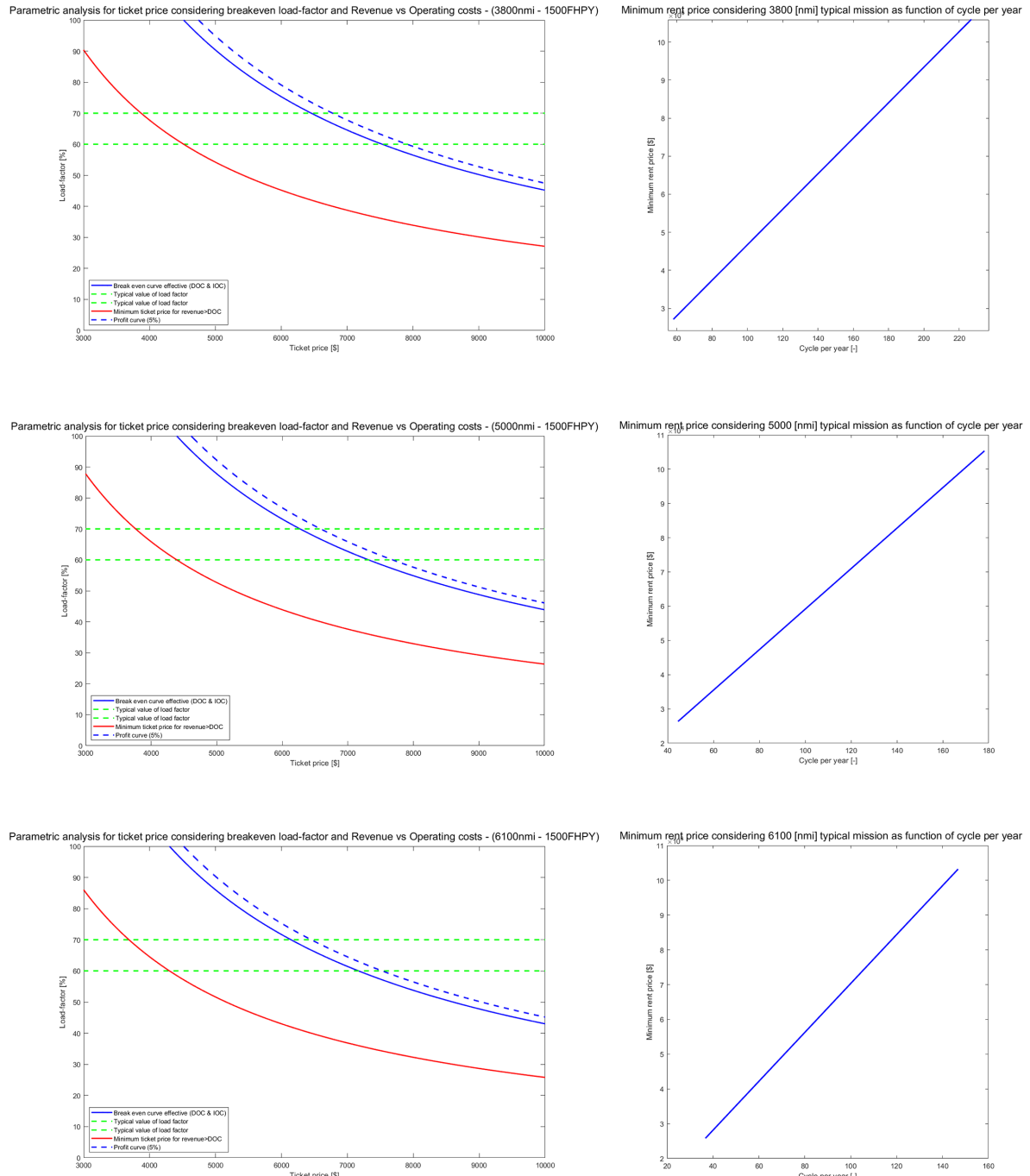


Figure 5.15: Plots obtained from cost analysis

By setting the typical range as that of type 1, corresponding to 3800 nmi, we also investigated the effects of the number of flight hours per year as follows in the figure 5.16.

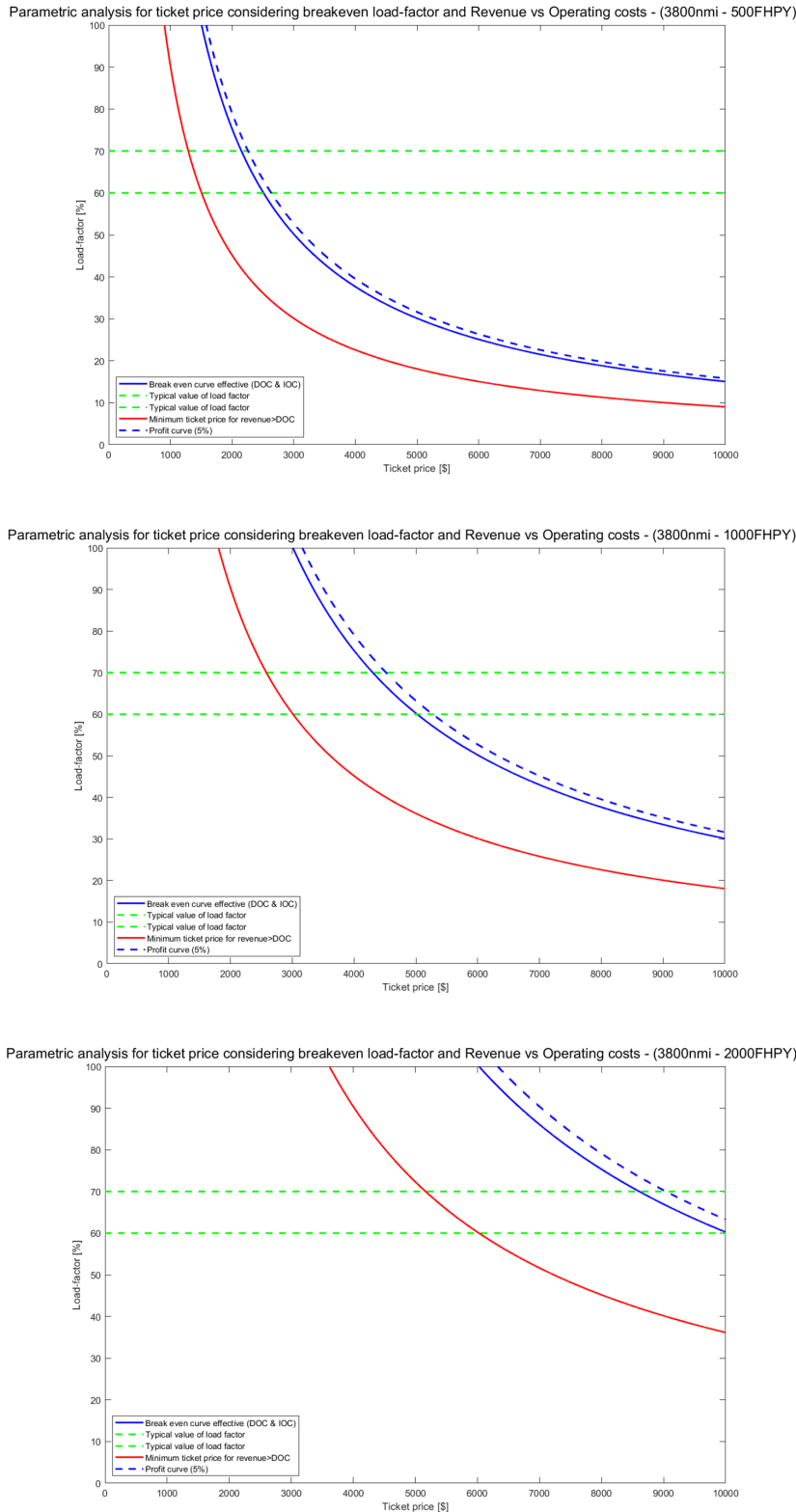


Figure 5.16: Plots of cost analysis varying the number of flight hours per year with typical range at 3800nmi

Chapter 6

Performance

At this point in the conceptual design, where the fundamental dimensions of the aircraft and its main components are defined, together with the results of the aerodynamic analyses carried out, it is possible to perform a performance analysis in order to validate the sizing carried out and verify that the required performance is actually met.

In the following paragraphs, the fundamental mission segments (takeoff, climb, cruise and landing) will be analysed. The approach used is based on the classical theory of flight mechanics; the equations already used in the wing loading section will therefore be used. A conceptual difference behind the performance analysis, compared to the sizing, is the unknown to be found:

- in dimensioning, the criteria to be met provide the input data and the aircraft characteristics are the results;
- in performance analysis, the aircraft characteristics are the input data, while the output of the process constitutes what, theoretically, the aircraft is capable of doing.

The final step in each stage analysed will be to compare the results obtained with the performance set. Although it may seem trivial to carry out the reverse of the procedure already used for sizing, it is necessary to observe that the data relative to aerodynamics, in the sizing phase, were based on a series of preliminary estimates based on historical records or general considerations, while the current data come from results, although also based on simplified calculation models, relative to calculations carried out on the sized aircraft.

6.1 Takeoff

The first phase analysed is the takeoff phase. At this stage, it is necessary to estimate in a more precise way the contribution of high-lift devices on the maximum lift coefficient, expressed as $\Delta C_{l_{max}}$ since, as already specified, the aerodynamic analysis was carried out using the clean configuration. So in addition to carrying out the actual performance analysis, at this stage, it was determined the minimum $\Delta C_{l_{max}}$ required to ensure compliance with take-off performance, hence TODR, and to guarantee an adequate stall speed. The lower the

$\Delta C_{l_{max}}$, the simpler and more economical the configuration of the high-lift devices will be. Based on the required increment, it is possible to choose the best configuration of flaps and slats required, using the table provided by Raymer, which associates a certain $\Delta C_{l_{max}}$ with each type of device. A suitable value was found using $\Delta C_{l_{max}} = 1.5$ after a series of attempts. Entering the Raymer table with this value, we opted for slotted flaps combined with leading edge fixed slots. This combination gives a value of $1.3 + 0.2 = 1.5$, which is quite close to the minimum found, also because for takeoff flap settings, lift increments of 60% has been used, for the reasons specified in section 3.2.1. The slotted flap is a plain flap with a slot between



Figure 6.1: Slotted flap and leading-edge slot configuration

the wing and the flap. This permits high-pressure air from beneath the wing to exit over the top of the flap, which tends to reduce separation. This increases lift and reduces drag. The leading-edge slot is simply a hole that permits high-pressure air from under the wing to blow over the top of the wing, delaying separation and stall. Usually such a slot is fixed, but might have closing doors to reduce drag at high speeds. Leading-edge devices alone do little to improve lift for takeoff and landing because they are effective only at fairly high angles of attack. However, they are very useful when used in combination with trailing-edge flaps because they prevent premature airflow separation caused by the flaps. An interesting result is that in the preliminary stage, where not much was known about the aerodynamic data, a high-lift device configuration consisting of double slotted flaps and slats was assumed. It was realized that such a configuration provided an excessive increase in $C_{L_{max}}$ compared to that required, so choosing this architecture would have been an unnecessary aggravation in terms of complexity and cost, and also required volumes within the wings. In a complex context such as aircraft design, simplicity and essentiality, within the limits of what is possible, is always a good choice.

The key parameters used to analyse the take-off phase were then recalculated based on the new known data. The equations used have been avoided in this section as they are already present in the section where the wing loading was derived. It can be seen that performance parameters such as runway length at take-off and stall speed are completely acceptable and realistic values. Moreover, the calculations were repeated for more severe take-off conditions, that is, for an airport at 5000 ft above sea level on a hot day. This results in a σ of 0.792 and a scaled-down T/W , considering the loss of thrust due to the increase in altitude. Again, the TODR specification is met, provided the takeoff load factor is increased slightly by 25%. This confirms that the aircraft can also take off from airports with worse conditions than sea level. The significant results of this analysis are shown in the table 6.1.

Parameter	Symbol	Value (BE)	Value (SI)
Maximum lift coeff.	$C_{L_{max,to}}$	2.1	2.1
Parasite drag	$C_{D0_{to}}$	0.083	0.083
Induced drag factor	K_{to}	0.08	0.08
Load factor standard AP	n_z	1.15	1.15
Load factor worst AP	n_z	1.44	1.44
Stall speed standard AP	V_{st}	110.7 kn	56.95 m/s
Stall speed worst AP	V_{st}	124.2 kn	63.9 m/s
TODR standard AP	$TODR$	4301 ft	1311 m
TODR worst AP	$TODR$	5073 ft	1546 m

Table 6.1: Main takeoff performance parameters

6.2 Climb

Similar calculations were performed for the climb phase as for the wing-loading phase. In particular, new aerodynamic data from RDS analyses were used, from which the new maximum climb efficiency could be calculated. The wing loading and T/W ratio, which were the unknowns in the sizing phase, are now given. The wing loading has been scaled to the weight in the climb phase.

The performance criterion for this step is that the climb gradient with an inoperative motor must be greater than or at most equal to the minimum gradient required by the regulations, which is always 0.012. The new performance calculations showed a value of $G_{OEI} = 0.102$ then the requirement is fulfilled.

Lastly, it was decided to determine the new climb rates and the new rate of climb, in order to compare them with those chosen at the sizing stage. It should be noted that these performances were not given in the specification, however it was decided to ensure that they were still in an acceptable range. The values obtained are shown in table 6.2 (together with the other characteristic values for the climb) and considering that the assumed values were 250 kn and 3100 ft/min, it can be considered satisfactory.

Parameter	Symbol	Value (BE)	Value (SI)
Lift coefficient	$C_{L_{cl}}$	0.9	0.9
Parasite drag	$C_{D0_{cl}}$	0.0323	0.0323
Induced drag factor	K_{cl}	0.052	0.052
Climb Efficiency	E_{cl}	12.02	12.02
Climb speed	V_{cl}	223 kn	114.7 m/s
Rate of Climb	RoC	2953 ft/min	900 m/min
Wing loading	$(W/S)_{cl}$	89.84 lb/ft ²	4302 N/m ²
Climb gradient OEI	G_{OEI}	0.102	0.102

Table 6.2: Main climb performance parameters

6.3 Cruise

As for the cruise phase, the Breguet equations were used to calculate the range. It should be noted that these equations are based on the assumption of constant C_L and cruise speed, a condition that is not entirely accurate and provides an overestimate of the actual capabilities. The values needed for the calculation and the performance data obtained are shown below from which it emerges that the cruise requirement is found to be satisfied.

Parameter	Symbol	Value (BE)	Value (SI)
Cruise speed	V_{cr}	459 kn	236.1 m/s
Efficiency in cruise	$E_{cr,mean}$	17	17
Range	R_{cr}	6554 nm	12138 km

Table 6.3: Main cruise performance parameters

6.4 Landing

Also for the landing phase, the calculation of the required runway length for landing was based on the flight mechanics equations. All terms and equations used are avoided as they are already explained in the section 3.2.5. Also for this last phase, the necessary aerodynamic data were extrapolated and $\Delta C_{l_{max}}$ results from the takeoff performance calculation were used, in this case considering its full value without decreasing coefficients for the reasons already stated. The necessary data and the results obtained are shown below in 6.4. Again, the results obtained are satisfactory.

Parameter	Symbol	Value (BE)	Value (SI)
Maximum lift coeff.	$C_{L_{max,lnd}}$	2.7	2.7
Parasite drag	$C_{D0,lnd}$	0.1028	0.1028
Induced drag factor	K_{lnd}	0.06	0.06
Landing Efficiency	E_{lnd}	4.95	4.95
Drag coefficient	$C_{D_{lnd}}$	0.54	0.54
Touch down speed	V_{td}	87.81 kn	45.2 m/s
Landing distance	LD	2900 ft	884 m

Table 6.4: Main landing performance parameters

List of Figures

1.1	World passenger traffic evolution, 1945-2022, ICAO data	4
1.2	Business jet market size by region, 2018-2030, Polaris Market data	5
2.1	Sizing mission profile	9
2.2	W_0 in lb as a function of AR and engine technological level - 3D plot	12
2.3	W_0 , W_{fuel} and W_{empty} in lb as a function of AR for desidered engine technological level (2015) ($C_T = 0.525 \text{ } h^{-1}$)	12
2.4	W_0 , W_{fuel} and W_{empty} in lb as a function of engine technological level for AR=10	13
3.1	High-Bypass Turbofan characteristic curves as a function of flight altitude and Mach number	16
3.2	Wing sweep historical trend	17
3.3	Maximum lift coefficient as a function of sweep angle	18
4.1	Tail off pitch-up boundaries	29
4.2	Effect of sweep on desired taper ratio	29
4.3	Thickness ratio historical trend	31
4.4	Effect of t/c on maximum lift	31
4.5	Initial tail sizing	34
4.6	Chosen configuration for engine	36
4.7	Tricycle landing-gear geometry	37
4.8	Main dimension parameters of the oleo strut shock absorber	38
4.9	Orthographic view	40
4.10	Top view	41
4.11	Side view	42
4.12	Front view	43
4.13	Isometric view	44
5.1	Aerodynamics RDS data: Conventional airfoil method (FPS units)	45
5.2	Some RDS C_D0 aerodynamics results	46
5.3	C_D0 vs Mach number plot for different flight altitudes	47
5.4	Induced Drag Factor (K) plot	48
5.5	Oswald's efficiency plot	49

LIST OF FIGURES

5.6	Lift curve slope and $C_{L_{max}}$ vs Mach Number	49
5.7	Lift-to-drag at sea level	50
5.8	Lift-to-drag at 40000 ft	50
5.9	Lift-to-drag in level flight (36000 ft) at initial cruise condition	51
5.10	Lift-to-drag in level flight (36000 ft) at final cruise condition	51
5.11	Drag polar at sea level	52
5.12	Drag polar at 40000 ft	52
5.13	Element of life-cycle cost	53
5.14	Typical mission considered	60
5.15	Plots obtained from cost analysis	62
5.16	Plots of cost analysis varying the number of flight hours per year with typical range at 3800nmi	63
6.1	Slotted flap and leading-edge slot configuration	65

List of Tables

1.1	Initial requirements	5
1.2	Long range business jets data collection	6
1.3	Reference aircraft: Gulfstream G650ER specs	6
2.1	Regression exponents for jet transport aircraft	7
2.2	Historical mission segment weight fractions for a business jet	9
2.3	Mission segment weight fraction	14
2.4	Main results of preliminary sizing	14
3.1	Takeoff wing loading main results	20
4.1	Refined mission segment weight fraction	26
4.2	Main results of refined sizing	26
4.3	Gulfstream G650ER vs Scorpion MZ Aircraft comparison of main parameters	27
4.4	Wing parameters	31
4.5	Horizontal tail parameters	34
4.6	Vertical tail parameters	35
5.1	First parameters chosen for cost estimation	54
5.2	Total hours of work	55
5.3	Wrape rates	55
5.4	Labour costs	55
5.5	Other costs	56
5.6	Typical mission #1 cost results	61
5.7	Typical mission #2 cost results	61
5.8	Typical mission #3 cost results	61
6.1	Main takeoff performance parameters	66
6.2	Main climb performance parameters	66
6.3	Main cruise performance parameters	67
6.4	Main landing performance parameters	67

Bibliography

- [1] Daniel P. Raymer, *Aircraft design: A conceptual approach, 1st edition*, AIAA educational series, 1987.
- [2] Jack D. Mattingly, William H. Heiser, David D. Pratt, *Aircraft Engine Design, 2nd edition*, AIAA educational series, 2002.
- [3] Ajoy K. Kundu, *Aircraft design*, Cambridge aerospace series, 2010.
- [4] Lloyd R. Jenkinson, James F. Marchman III, *Aircraft design projects for engineering students*, Butterworth-Heinemann, 2003.
- [5] Ebgert Torenbeek, *Advanced aircraft design: conceptual design, analysis and optimization of subsonic civil airplanes*, John Wiley & Sons, 2013.